1

Review of Soil Mechanics Concepts and Analytical Techniques Used in Foundation Engineering

Manjriker Gunaratne

CONTENTS

1.1 Introduction

Geotechnical engineering is a branch of civil engineering in which technology is applied to the design and construction of structures involving geological materials. Earth's surface material

consists of soil and rock. Of the several branches of geotechnical engineering, soil and rock mechanics are the fundamental studies of the properties and mechanics of soil and rock, respectively. Foundation engineering is the application of the principles of soil mechanics, rock mechanics, and structural engineering to the design of structures associated with earthen materials. On the other hand, rock engineering is the corresponding application of the above technologies to the design of structures associated with rock. It is generally observed that most foundation types supported by intact bedrock present no compressibility problems. Therefore, when designing common foundation types, the foundation engineer's primary concerns are the strength and compressibility of the sub-surface soil and whenever applicable, the strength of bedrock.

1.1.1 Origin of Geomaterials

The earth's interior consists of a core, mantle, and outer crust. The core is made up of a solid inner part and a liquid outer part existing at extremely high temperatures and pressures. The mantle consists of harder material under relatively cooler temperatures.

The outer zone of the mantle and the inner zone of the outer crust are made up of a dense, semisolid or plastic rock layer known as the asthenosphere. The outer crust or the lithosphere (rock sphere) contains hard brittle rock topped at most locations by the soil overburden or oceans and soil overburden.

The lithosphere is not formed as one continuing crust but rather constitutes a number of tectonic plates that constantly move somewhat independently of each other. Plate divergence at the boundaries produces rifts that allow molten material from the asthenosphere to rise, cool, and create new lithosphere. These locations generally coincide with areas of volcanic activity. On the other hand, plate convergence at the boundaries causes constant stress buildup, creating conditions for possible earthquakes.

A foundation engineer needs to be informed of two aspects of the above discussion. The primary information relates to the formation of the soil overburden. Gradual weathering of the rock material in the lithosphere due to physical means (i.e., pressure and temperature related), chemical means, or man's action can create distinct stages of decomposition. Ideally, successive *in situ* staged decomposition of rock would result in boulders, gravel, sand silt, and clay. The most important information that a foundation engineer must have regarding the site selected for a given building is the classification of soil type (Section 1.2) and the condition of bedrock (decomposed or solid). The secondary information pertains to the seismicity of the general geographical area. If the area is known to be seismically active, then principles of soil dynamics must also be incorporated in foundation design (Sections 3.6 and 3.7).

1.2 Soil Classification

1.2.1 Mechanical Analysis

According to texture or the "feel," two different soil types can be identified. They are (1) coarse-grained soil (gravel and sand) and (2) fine-grained soil (silt and clay). Whereas the engineering properties (primarily strength and compressibility) of coarse-grained soils depend on the size of individual soil particles, the properties of fine-grained soils are mostly governed by the moisture content. Hence, it is important to identify the type of soil at a given construction site because the most effective construction procedures depend on the soil type. Geotechnical engineers use a

universal format called the Unified Soil Classification System (USCS) to identify and label soil. This system is based on the results of common laboratory tests of mechanical analysis and Atterberg limits.

In classifying a soil sample retrieved from a given site, mechanical analysis is conducted in two stages: (1) sieve analysis for the coarse fraction (gravel and sand) and (2) hydrometer analysis for the fine fraction (silt and clay). Of these, sieve analysis is conducted according to ASTM (American Society for Testing and Materials) D421 and D422 procedures, using a set of U.S. standard sieves (Figure 1.1); the most commonly used sieves are U.S. Standard numbers 20, 40, 60, 80, 100, 140, and 200, which correspond to sieve openings of 0.85, 0.425, 0.25, 0.18, 0.15, 0.106, and 0.075 mm, respectively. During the test, the percentage (by weight) of the soil sample retained on each sieve is recorded, from which the percentage (*R*%) passing (or finer than) a given sieve size (D) is determined.

On the other hand, if a substantial portion of the soil sample consists of fine-grained soils (D < 0.075 mm), then sieve analysis has to be followed by hydrometer analysis (Figure 1.2). The latter test is performed by first treating the "fine fraction" with a deflocculating agent such as sodium hexa-meta-phosphate (Calgon) or sodium silicate (water glass) for about half a day and then allowing the suspension to settle in a hydrometer jar maintained at a constant temperature. As the heavier particles settle, followed by the lighter ones, a calibrated ASTM 152H hydrometer is used to estimate the fraction (percentage, R%) by weight still settling above the hydrometer bottom at any given stage. Furthermore, the particle size (*D*) that has settled past the hydrometer bottom at that stage in time can be estimated from the well-known Stokes' law for settling of objects in a liquid. It is realized that R% is the weight percentage of soil finer than D.

Further details of the above tests such as the correction to be applied to the hydrometer reading and determination of the effective length of the hydrometer are provided by Bowles (1986) and Das (2002). For soil samples that have significant coarse and fine fractions, both sieve and hydrometer analysis results (*R*% and *D*) can be logically combined to generate grain (particle) size distribution (PSD) curves such as those indicated in Figure 1.3. As an example, in Figure 1.3, it can be seen that 30% of soil type A is finer than 0.075 mm (U.S. No. 200 sieve), with *R%* = 30 and *D* = 0.075 mm being the last pair of results obtained from sieve analysis. In combining sieve analysis data with hydrometer analysis data, one has to convert the R% (based on the fine fraction only) and *D* (size) obtained from hydrometer analysis to percent passing based on the weight of the entire sample, in order to ensure the continuity of the PSD curve. As an example, let the results from one hydrometer reading of soil sample A be *R%* = 90 and *D* = 0.05 mm. To plot the curve, one needs the percentage of the entire sample finer than 0.05 mm. Since what is finer than 0.05 mm is 90% of the fine fraction (30% of the entire sample) used for hydrometer analysis, the converted percent passing for the final plot can be obtained by multiplying 90% by the fine fraction of 30%. Hence, the converted data used to plot Figure 1.3 are percent passing = 27 and *D* = 0.05 mm.

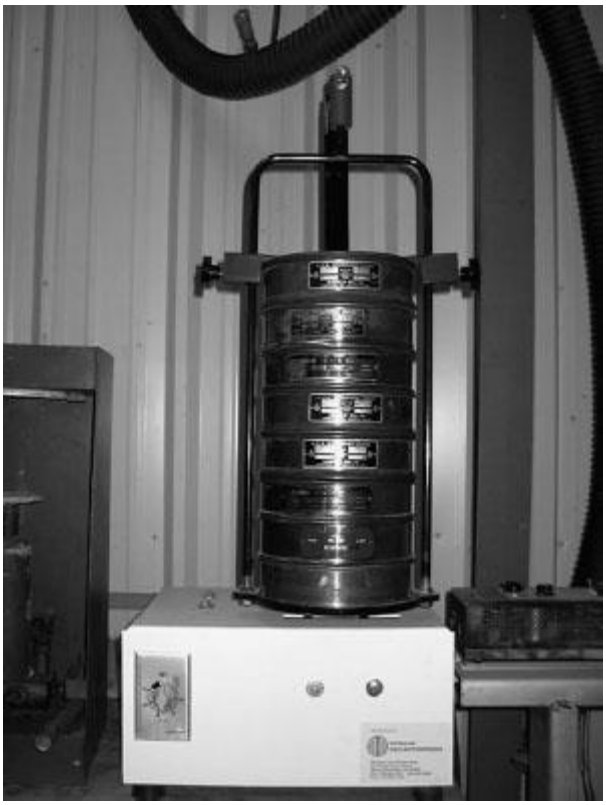

FIGURE 1.1
Equipment used for sieve analysis. (Courtesy of the University of South Florida.)

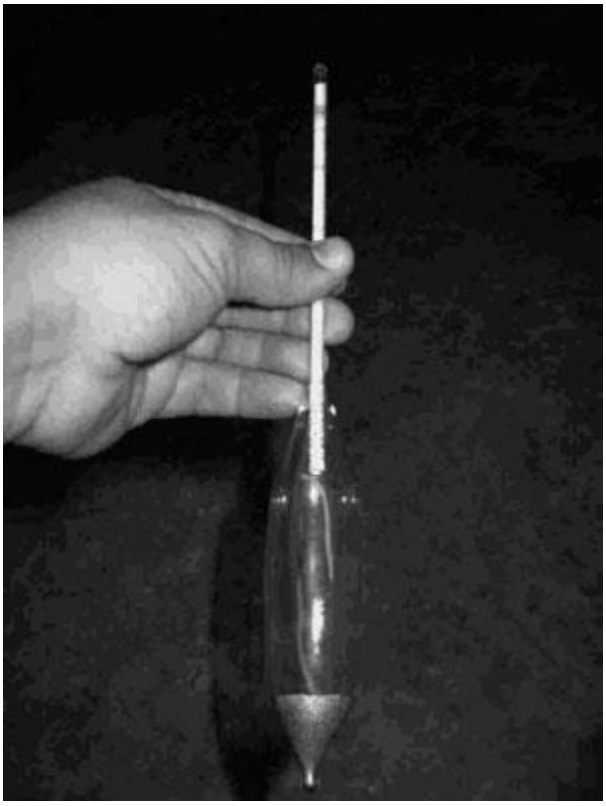

FIGURE 1.2
Equipment used for hydrometer analysis. (Courtesy of the University of South Florida.)

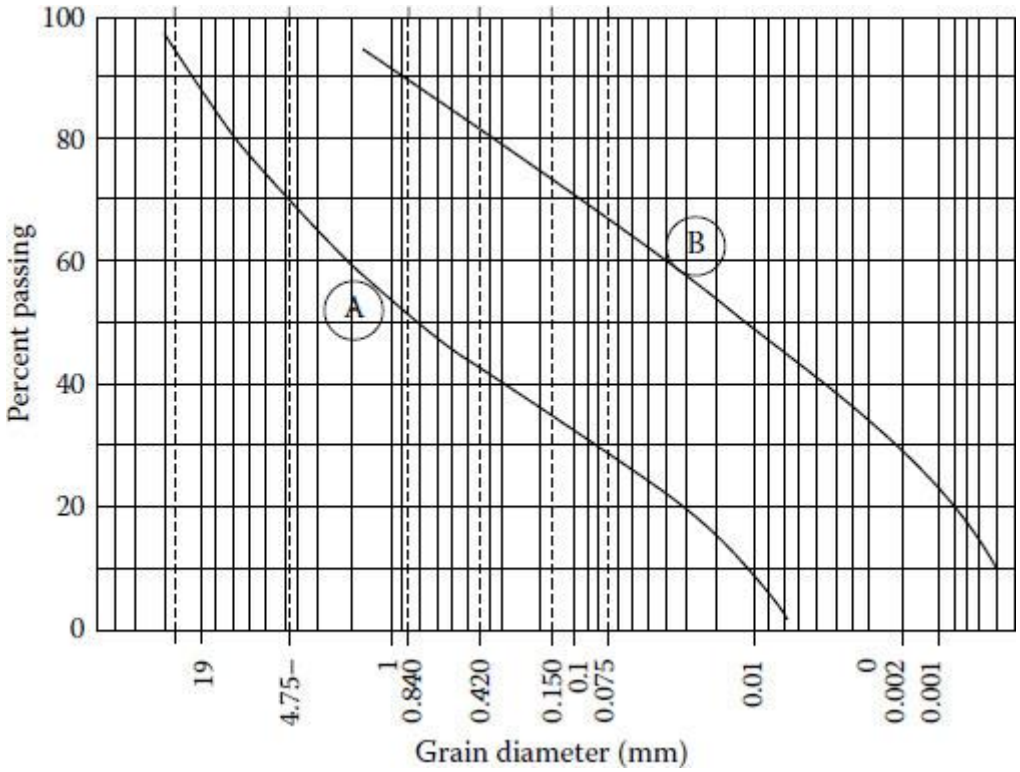

FIGURE 1.3

Grain (particle) size distribution curves. (From Edward Nawy (ed.), *Concrete Design Handbook*, Taylor & Francis, Boca Raton, FL, 1997.)

1.2.2 Atterberg Limits

As mentioned previously, the properties of fine-grained soils are governed by water. Hence, the effect of water must be the primary consideration in classification of fine-grained soils. This is achieved by using the Atterberg limits or consistency limits. The physical state of a fine-grained soil changes from brittle to liquid state with increasing water content, as shown in Figure 1.4.

Theoretically, the plastic limit (PL) of a soil is defined as the water content at which the soil changes from "semisolid" to "plastic" (Figure 1.4). For a given soil sample, this is an inherent property of the soil, which can be determined by rolling a plastic soil sample into a worm shape in order to gradually reduce its water content by exposing more and more of an area until the soil becomes semisolid in consistency. This change can be detected by cracks appearing on the sample. According to ASTM 4318, the PL is the water content at which cracks develop on a rolled soil sample at a diameter of 3 mm. Thus, the procedure to determine the PL is one of trial and error. While the apparatus (ground glass plate and moisture cans) used for the test is shown in Figure 1.5, the reader is referred to Bowles (1986) and Das (2002) for more details.

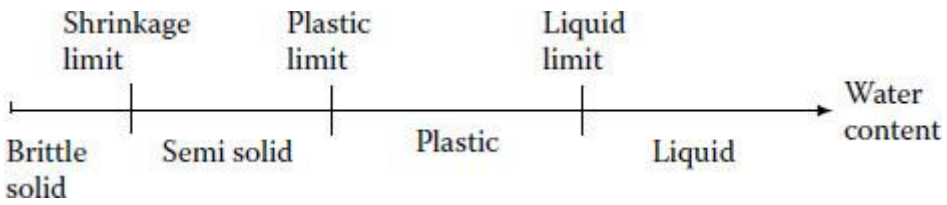

FIGURE 1.4

Variation of the fine-grained soil properties with the water content.

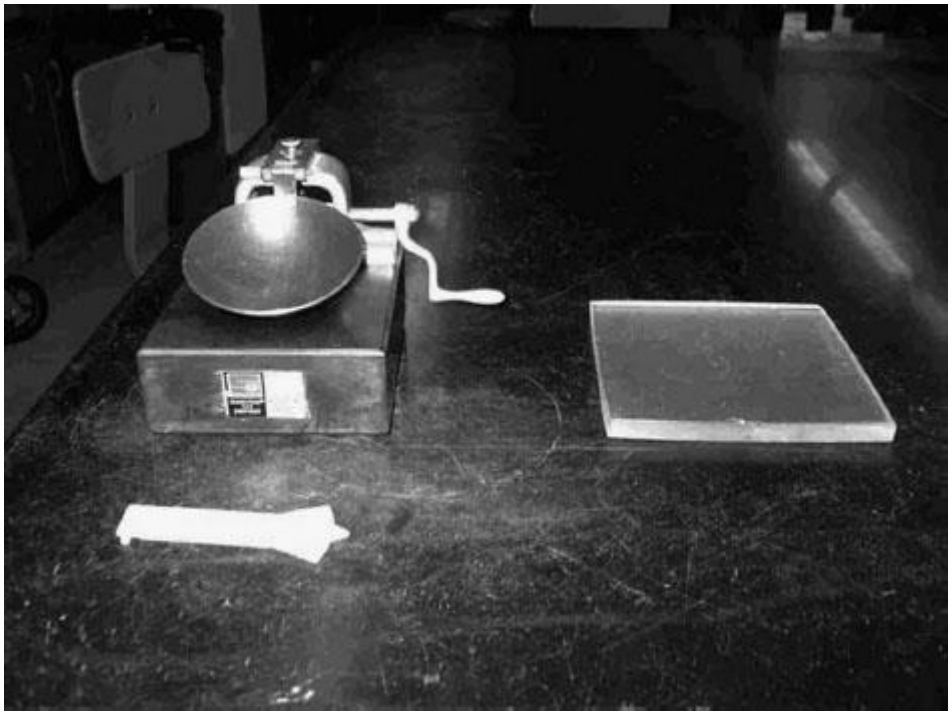

FIGURE 1.5
Equipment for the plastic limit-liquid limit tests. (Courtesy of the University of South Florida.)

On the other hand, the liquid limit (LL), which is visualized as the water content at which the state of a soil changes from "plastic" to "liquid" with increasing water content, is determined in the laboratory using the Casagrande liquid limit device (Figure 1.5). This device is specially designed with a standard brass cup on which a standard-sized soil paste is applied during testing. In addition, the soil paste is grooved in the middle by a standard grooving tool thereby creating a "gap" with standard dimensions. When the brass cup is made to drop through a distance of 1 cm on a hard rubber base, the number of drops (blows) required for the parted soil paste to come back into contact through a distance of 1/2 in is counted. Details of the test procedure can be found in the work of Bowles (1986) and Das (2002). ASTM 4318 specifies LL as the water content at which the standard-sized gap is closed in 25 drops of the cup. Therefore, one has to repeat the experiment for different trial water contents, each time recording the number of blows required to fulfill the closing condition of the soil gap. Finally, the water content corresponding to 25 blows (or the LL) can be interpolated from the data obtained from all trials. The plasticity index (PI), which is a widely used parameter for the classification of fine-grained soils, is evaluated as follows:

$$PI = LL - PL \tag{1.1}$$

1.2.3 Unified Soil Classification System

In the commonly adopted USCS shown in Table 1.1, the aforementioned soil properties are used effectively to classify soils. Example 1.1 illustrates the classification of the two soil samples A and B represented by the PSD curves shown in Figure 1.3. Definition of the following two curve parameters is necessary to accomplish the classification:

TABLE 1.1

Unified Soil Classification System

Division		Description	Group Symbol	Identification	Laboratory Classification Criteria
More than 50% soil retained in U.S. 200 sieve (0.075 mm)	More than 50% retained in U.S. No. 4 (4.75 mm)	Clean gravels	GW	Well-graded gravels	$C_u > 4,1 < C_c < 3$
		GP	Poorly graded gravels	Not meeting GW criteria	
		Gravel with fines	GM	Silty gravel	Falls below A line in the plasticity chart, or PI less than 4
	More than 50% passing U.S. No. 4 (4.75 mm)	Clean sand	GC sw	Clayey gravel Well graded sand	Falls above A line in the plasticity chart, or PI greater than 7 $C_u > 4,1 < C_c < 3$
			SP	Poorly graded sand	Not meeting SW criteria
		Sand with fines	SM	Silty sand	Falls below A line in the plasticity chart, or PI less than 4
More than 50% soil passing U.S. 200 sieve (0.075 mm)	Fine-grained soils (LL < 50)		SC ML	Clayey sand Inorganic silts with low plasticity	Falls above A line in the plasticity chart, or PI greater than 7
			CL	Inorganic clays with low plasticity	
			OL	Organic clays / silts with low plasticity	
	Fine-grained soils (LL > 50)		MH	Inorganic silts with high plasticity	
			CH OH	Inorganic clays with high plasticity	
Highly organic soils			Pt	Organic clays / silts with low plasticity	Use the Casagrande plasticity chart shown above

Source: R.D. Holtz and W.D. Kovacs, *An Introduction to Geotechnical Engineering*, Prentice Hall, Inc., Engelwood Cliff NJ, 1981, with permission.

Coefficient of uniformity $(C_u) = D_{60}/D_{10}$

Coefficient of curvature $(C_c) = D_{30}^2/D_{60}D_{10}$

where D_i is the diameter corresponding to the *i*th percent passing on the PSD.

Example 1.1

Classify soils A and B with PSD curves shown in Figure 1.3.

Solution

Soil A. The percentage of coarse-grained soil is approximately equal to 70% (=100% – 29%). It must be noted that 29% is the percent passing corresponding to 0.075 mm size designated as the U.S. No. 200 sieve size and the lower threshold size of coarse-grained soils. Therefore, A is a coarse-grained soil. The percentage of sand in the coarse-fraction is equal to (70 – 29)/70 × 100 = 57%. It must be noted that 70% is the percent passing corresponding to 4.75 mm size designated as the U.S. No. 4 sieve size and the upper threshold size of sands. Thus, according to the USCS (Table 1.1), Soil A is sand. If one assumes a clean sand, then

$C_c = (0.075)^2/(2 \times 0.013) = 0.21$, does not meet the criterion for SW
$C_u = (2)/(0.013) = 153.85$, meets criterion for SW

Hence, soil A can be classified as a poorly graded sand designated as SP.

Soil B. The percentage of coarse-grained soil is equal to 32% (=100% – 68%). Hence, B is a fine-grained soil. Assuming that LL and PL are equal to 45 and 35, respectively (which results in a PI value of 10 from Equation 1.1), using *Casagrande's plasticity chart* (Table 1.1) soil B can be classified as silty sand with clay (ML).

1.3 Water in Soils

1.3.1 Clay Minerals

Mechanical weathering described in Section 1.1.1 tends to produce coarse-grained soils such as boulders, cobbles, gravels, and sands, whereas chemical weathering produces clay minerals. The engineering behavior, which is primarily described by the strength and compressibility characteristics, of coarse-grained soils is mainly dependent on the grain-size distribution and the degree of packing. On the other hand, in clay minerals that are electrochemically active, the water content has a significant bearing on the engineering behavior.

Clay minerals are hydrous aluminum silicates that contain metallic ions such as Si^{2+}, Al^{2+}, Mg^{2+}, or Fe^{2+}. X-ray diffraction studies (Holtz and Kovacs, 1981) have revealed that the crystals of the above minerals consist of many crystal sheets having a repeating atomic structure. The two fundamental crystal sheets are tetrahedral silica and octahedral alumina. As shown in Figure 1.6a, the silica tetrahedral unit consists of four oxygen atoms at the corners surrounding a silicon atom. Similarly, in the octahedral alumina unit, six oxygen atoms or hydroxyls (OH) surround a metallic atom such as Al or Mg (Figure 1.6b).

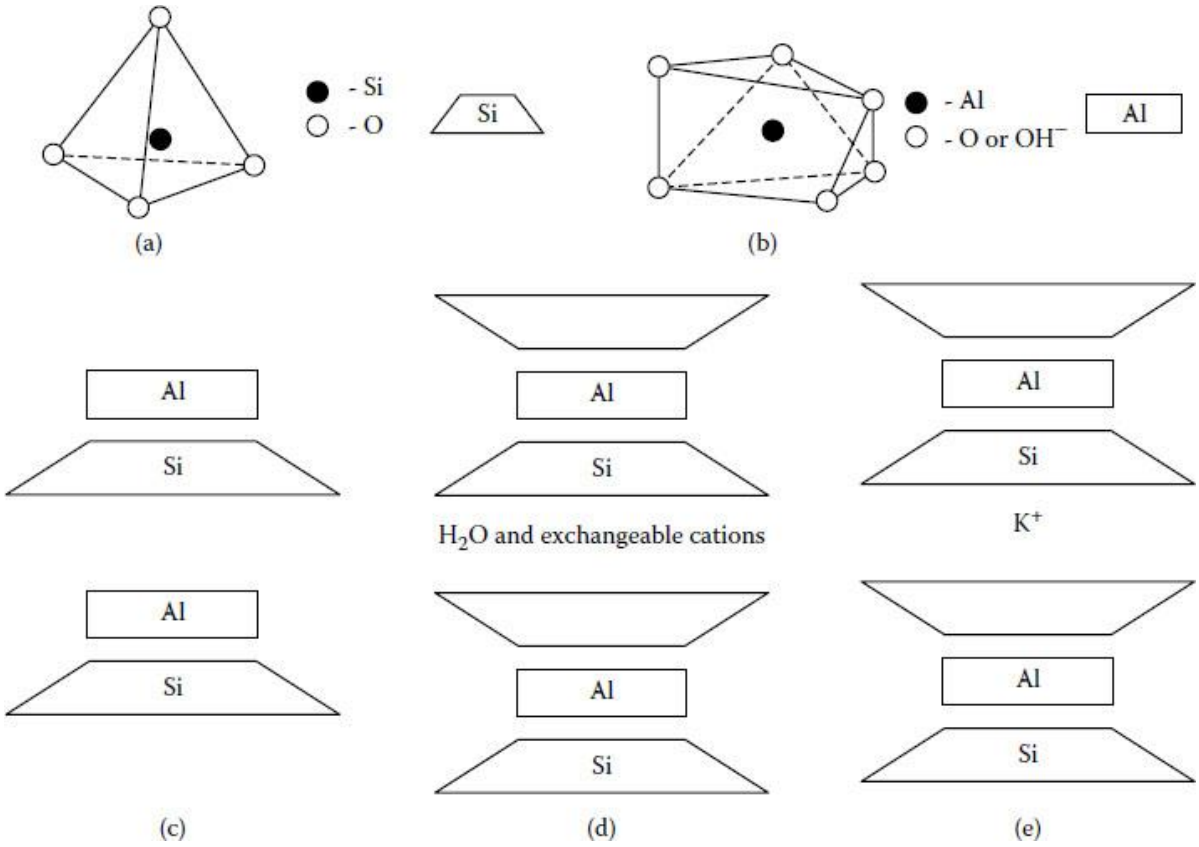

FIGURE 1.6

(a) Tetrahedral silica. (b) Octahedral alumina. (c) Basic kaolinite crystal structure. (d) Basic montmorillonite crystal structure. (e) Basic illite crystal structure.

An example of a 1:1 clay mineral is kaolinite with the basic crystal structure shown in Figure 1.6 c. The tetrahedral and octahedral units share common oxygen atoms, whereas hydrogen bonding holds the successive layers together. The absence of interchangeable cations in between the basic layers limits the influence of water on the engineering behavior of kaolinite.

Montmorillonite (Figure 1.6d) and illite (Figure 1.6e) are common examples of 2:1 clay minerals. In the montmorillonite crystal structure, the bonding between the silica sheets is relatively weak compared to the bonding between slica and alumina in kaolinite. Hence, polarized water molecules and exchangeable cations can easily enter the space between the two layers in large quantities and separate them, thus imposing a significant effect on the behavior of such clays. Consequently, subsurface soils with a significant content of montmo-rillonite clay mineral can induce damaging swelling pressures on superstructures and roads. The activity of montmorillonite clay minerals can be reduced by lime stabilization whereby the addition of Ca^{2+} into the interlayer space can reduce the water affinity of those minerals.

In illite (Figure 1.6e), on the other hand, the individual layers are tightly bonded with potassium ions K^{+}, thus disabling any water molecules intruding into the interlayer space. Hence, illite clay minerals do not exhibit swelling activity.

1.3.2 Effective Stress Concept

Voids (or pores) within the soil skeleton contain fluids such as air, water, or other contaminants. Hence, any load applied on a soil is partly carried by such pore fluids in addition to being borne by

the soil grains. Therefore, the total stress at any given location within a soil mass induced by loading can be expressed as the summation of the stress contributions from the soil skeleton and the pore fluids as

$$\sigma = \sigma' + u_p \tag{1.2}$$

where

σ = total stress (above atmospheric pressure)

σ' = stress in the soil skeleton (above atmospheric pressure)

u_p = pore (fluid) pressure (above atmospheric pressure)

The stress in the soil skeleton or the intergranular stress is also known as the *effective stress*, because it indicates that a portion of the total stress is carried by grain to grain contacts.

In the case of *dry soils* in which the pore fluid is primarily air, if one assumes that all pores anywhere within the soil is open to the atmosphere through interporous connectivity, Equation 1.2 infers that the effective stress would be the same as the total stress:

$$\sigma' = \sigma \tag{1.3}$$

On the other hand, in completely *wet* (*saturated*) *soils*, the pore fluid is mostly water and the effective stress at a given location is completely dependent on the *pore water pressure* (u_w). Then, from Equation 1.2,

$$\sigma' = \sigma - u_w \tag{1.4a}$$

Using the unit weights of soil (γ) and water (γ_w), Equation 1.4a can be modified to a more useful form as shown in Equation 1.4b.

$$\sigma'_v = \gamma z - \gamma_w d_w \tag{1.4b}$$

where

z = depth of the location from the ground surface (Figure 1.7)

d_w = depth of the location from the groundwater table (Figure 1.7) and water with a high degree of saturation (85% or above), Bishop and Blight (1963) showed that

A detailed discussion of the unit weights of soil is provided in Section 1.6. Finally, in *partly saturated soils*, the effective stress is governed by both the pore water pressure (u_w) and pore air pressures (u_a). For unsaturated soils containing both air

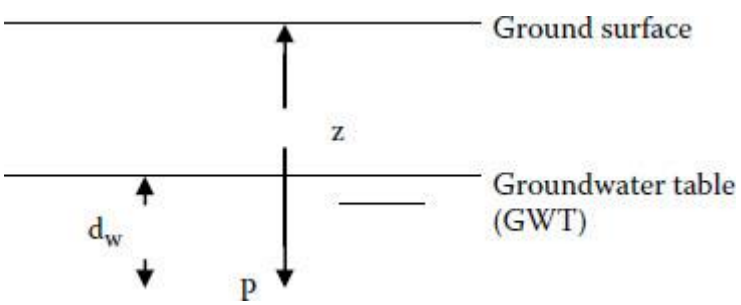

FIGURE 1.7

Illustration of *in situ* stresses.

$$\sigma = \sigma' + u_a - \chi(u_a - u_w), \tag{1.5}$$

where $(u_a - u_w)$ is the soil matric suction that depends on the surface tension of water and χ is a parameter in the range of 0 to 1.0 that depends on the degree of saturation. One can verify the applicability of Equation 1.4a for saturated soils based on Equation 1.5, since $\chi = 1$ for completely saturated soils.

1.4 Strength of Soils

The two most important properties of a soil that is of concern to a foundation engineer are strength and compressibility. Because earthen structures are not designed to sustain tensile loads, and soils have a tremendous compressive strength, the most common mode of soil failure is shearing. Hence, the shear strength of the foundation medium constitutes a direct input to the design of structural foundations.

1.4.1 Drained and Undrained Strengths

The shear strength of soils is assumed to originate from the strength properties of cohesion (c) and internal friction (#). Using Coulomb's principle of friction, the shear strength of a soil, τ_f, can be expressed as

$$\tau_f = c + \sigma_n \tan\Phi, \tag{1.6}$$

where σ_n is the normal stress on the failure plane. More extensive studies on stress–strain relations of soils (Section 1.9) indicate that more consistent and reliable strength parameters are obtained when Equation 1.6 is expressed with respect to the intergranular or the effective normal stress. Hence, c and # are also known as the effective strength parameters and are sometimes indicated as c' and #'. It is obvious that the strength parameters obtained from a shear strength test conducted under drained conditions would yield effective strength parameters because of the absence of pore water pressure. Hence, the effective strength parameters c' and #' are also termed the *drained strength* parameters. Failure loads computed based on effective or drained strength parameters are applicable in construction situations that either do not involve development of significant pore water pressures or where an adequate time elapses before construction is complete for dissipation of any pore pressures that could develop because of loading.

Effective strength parameters can also be obtained from any shear strength test conducted under undrained conditions if the pore water pressure developed during shearing is monitored accurately and Equation 1.6 is applied to estimate the shear strength in terms of the effective normal stress σ'_n. On the other hand, during any shear strength test conducted under undrained conditions, if Equation 1.6 is applied to estimate the shear strength in terms of the total normal stress σ_n, one would obtain an entirely different set of strength parameters c and #, which are called the total stress-based strength parameters. Using the concepts discussed in Section 1.9 and relevant stress paths, it can be shown that the total stress-based strength parameters are generally lower in magnitude than their effective strength counterparts.

From the discussion on soil strength, it is realized that the measured shear strength of a soil sample depends on the extent of pore pressure generation and therefore on the drainage condition that prevails during a shearing test. Hence, the type of soil and the loading rate expected during construction have an indirect bearing on the selection of the appropriate laboratory drainage condition that must be set up during testing.

A wide variety of laboratory and field methods are used to determine the shear strength parameters *c* and # of soils. The laboratory triaxial and direct shear testing and the *in situ* standard penetration testing (SPT), static cone penetration testing (CPT), and vane shear testing are the most common tests used to obtain foundation design parameters. The determination of the strength parameters using SPT and CPT is addressed in detail in Chapter 2. Hence, only the triaxial test based method of evaluating strength parameters will be discussed in this chapter.

1.4.2 Triaxial Tests

In this test, a sample of undisturbed soil retrieved from a site is tested under a range of cell (chamber, or confining) pressures that encompasses the expected field stress conditions imposed by the building foundation. Figure 1.8 shows the schematic diagram of the important elements of a triaxial setup, and the actual testing apparatus is shown in Figure 1.8b.

The pore pressure increase that can be expected during triaxial loading of a soil can be expressed using Skempton's pore pressure parameters, *A* and B, for that particular soil as

$$\Delta u = B\Delta\sigma_3 + A[\Delta\sigma_1 - \Delta\sigma_3], \tag{1.7}$$

where and $\Delta\sigma_1$ and $\Delta\sigma_3$ are the increments of the major and the minor principal stresses, respectively. It is seen from Figures 1.8a and b that, in triaxial tests, the major principal stresses generally happen to be the resultant vertical compression stress, which is composed of the axial (deviator) stress induced by the vertical ram load and the (vertical) confining pressure, whereas the minor principal stress is simply the (horizontal) confining pressure. When *A* and *B* parameters for a given soil types are determined using a set of preliminary triaxial tests, one would be able to predict the magnitude of the pore pressure that would be generated in that soil under any triaxial stress state. It can be shown that, for saturated soils, $B = 1.0$.

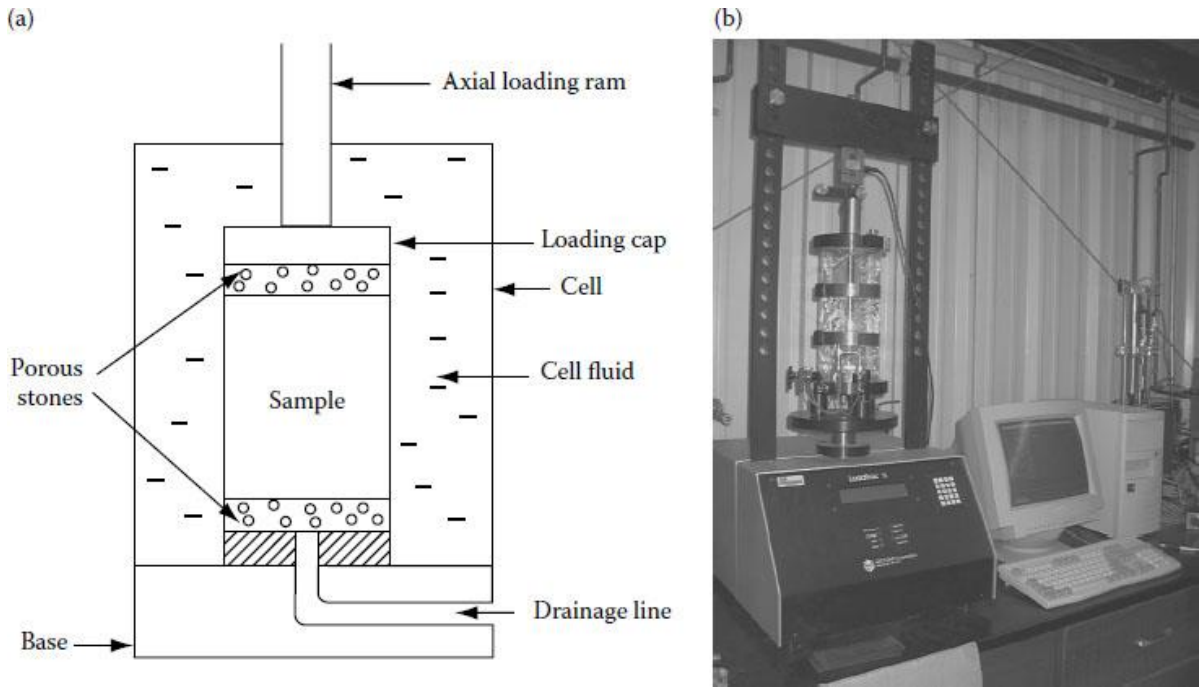

FIGURE 1.8

(a) Schematic diagram of triaxial test. (From Edward Nawy (ed.), *Concrete Design Handbook*, Taylor & Francis, Boca Raton, FL, 1997.) (b) Triaxial testing apparatus for soils. (Courtesy of the University of South Florida.)

An alternative way of expressing the pore pressure increase due to triaxial loading is as follows:

$$\Delta\sigma_{oct} + 3a\Delta\tau_{oct} \tag{1.8}$$

where a is the Henkel pore pressure parameter and $\Delta\sigma_{oct}$ and $\Delta\tau_{oct}$ are octahedral normal and octahedral shear stresses defined respectively as

$$\sigma_{oct} = [\sigma_1 + \sigma_2 + \sigma_3]/3 \tag{1.9a}$$

$$\tau_{oct} = [(\sigma_1 - \sigma_2)^2 + (\sigma_2 - \sigma_3)^2 + (\sigma_1 - \sigma_3)^2]^{1/2}/3 \tag{1.9b}$$

where σ_2 is the increment of the intermediate principal stress. Under the triaxial state of stress, the above expressions simplify to

$$\sigma_{oct} = [\sigma_1 + 2\sigma_3]/3 \tag{1.10a}$$

$$\tau_{oct} = [2(\sigma_1 - \sigma_3)]/3 \tag{1.10b}$$

With respect to the drainage condition used during testing, three types of triaxial tests can be conducted: (1) consolidated drained (CD) tests, (2) consolidated undrained (CU) tests, and (3) unconsolidated undrained (UU) tests. In CU and CD tests, before applying the axial compression, the above-mentioned confining pressure is applied by pressurizing the cell fluid to consolidate the soil sample back to the *in situ* effective stress state that existed before sampling. On the other hand, in the UU tests, the cell pressure is applied with no accompanying drainage or consolidation, simply to provide a confining pressure.

1.4.2.1 Triaxial Testing of Rocks

When foundations are designed on rock, as in the case of pile foundations driven to bed rock and pile and drilled shaft foundations cast on bedrock, an accurate estimate of the shear strength of the *in situ* rock is essential. A variety of methods are available in the literature (Goodman, 1989) to determine the shear strength of rock. Of these methods, the most accurate method of shear strength estimation is perhaps through triaxial testing. Triaxial testing is even more reliable for rock than for soils, because sampling-induced disturbance resulting in change of strength characteristics is not a major issue in the case of rocks. Moreover, correlations that have been developed between the shear strength of rock and the unconfined compression strength (Section 1.4.3) and the rock quality designation (RQD) also provide a convenient means of estimating the shear strength parameters of rock. Further details of such correlations are provided in Chapter 6 (Section 6.10). Triaxial testing of rock is performed using a special apparatus that can sustain the relatively large confining pressures often associated with rock and similarly large deviator stresses that must be applied on rock samples to induce shear failure. A set of such apparatus is illustrated in Figure 1.9a and b.

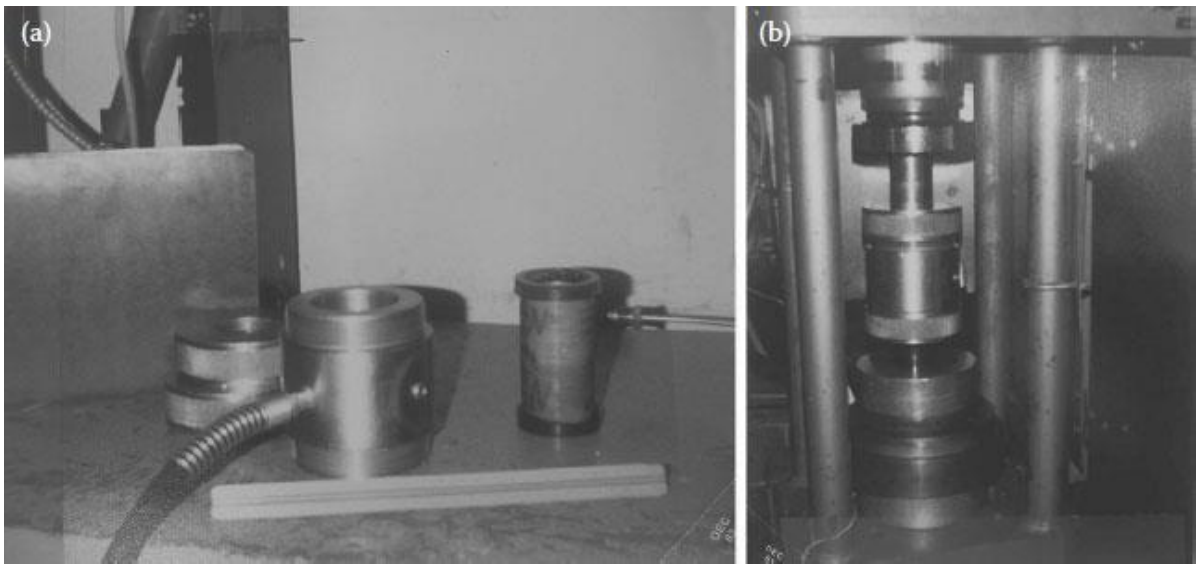

FIGURE 1.9

(a) Triaxial cell and membrane used in testing of rock samples. (b) Triaxial testing of rocks.

1.4.2.2 Selection of Triaxial Test Type Based on Construction Situation

The CD strength is critical in the consideration of long-term stability. Examples of such situations are

1. Slowly constructed embankment on a soft clay deposit
2. Earth dam under steady state seepage
3. Excavation of natural slopes in clay

On the other hand, CU strength is more relevant for the following construction conditions:

1. Raising of an embankment subsequent to consolidation under its original height
2. Rapid drawdown of a reservoir of an earthen dam currently operating under steady state seepage
3. Rapid construction of an embankment on a natural slope

Finally, the UU strength is applicable under conditions such as the following:

1. Rapid construction of an embankment over a soft clay
2. Large dam constructed with no change in water content in the clay core
3. Footing placed rapidly on a clay deposit

1.4.2.3 Computation of Strength Parameters Based on Triaxial Tests

Computations involving CU and UU tests are given in Examples 1.2 and 1.3, and the reader is referred to Holtz and Kovacs (1981) for more details on the testing procedures.

Example 1.2

Assume that two CU triaxial tests are conducted on a sandy clay sample from a tentative site in order to determine the strength properties. The applied cell pressures and the deviator stresses and measured pore pressures at failure are given in Table 1.2. The strength parameters can be estimated using the Mohr circle method as follows:

Solution

Total Strength Parameters. The total stresses (σ_1 and σ_3) acting on both test samples at failure are indicated in Figure 1.10a. Therefore, the Mohr circles for the two stress states can be drawn as shown in Figure 1.10c. Then, the total strength parameters (also referred to as the undrained strength parameters) can be evaluated from the slope of the direct common tangent, which is the Coulomb envelope (Equation 1.6) plotted on the Mohr circle diagram, as c = 4.0 kPa and # = 13.2°.

It is obvious that the generated pore pressure has been ignored in the above solution. The most appropriate applications of c and # obtained above are cases where foundations are rapidly constructed on well consolidated ground.

TABLE 1.2

Measured CU Triaxial Test Data

Test	Cell Pressure (kPa)	Deviator Stress at Failure (kPa)	Pore Pressure at Failure (kPa)
1	20	20.2	5.2
2	40	30.4	8.3

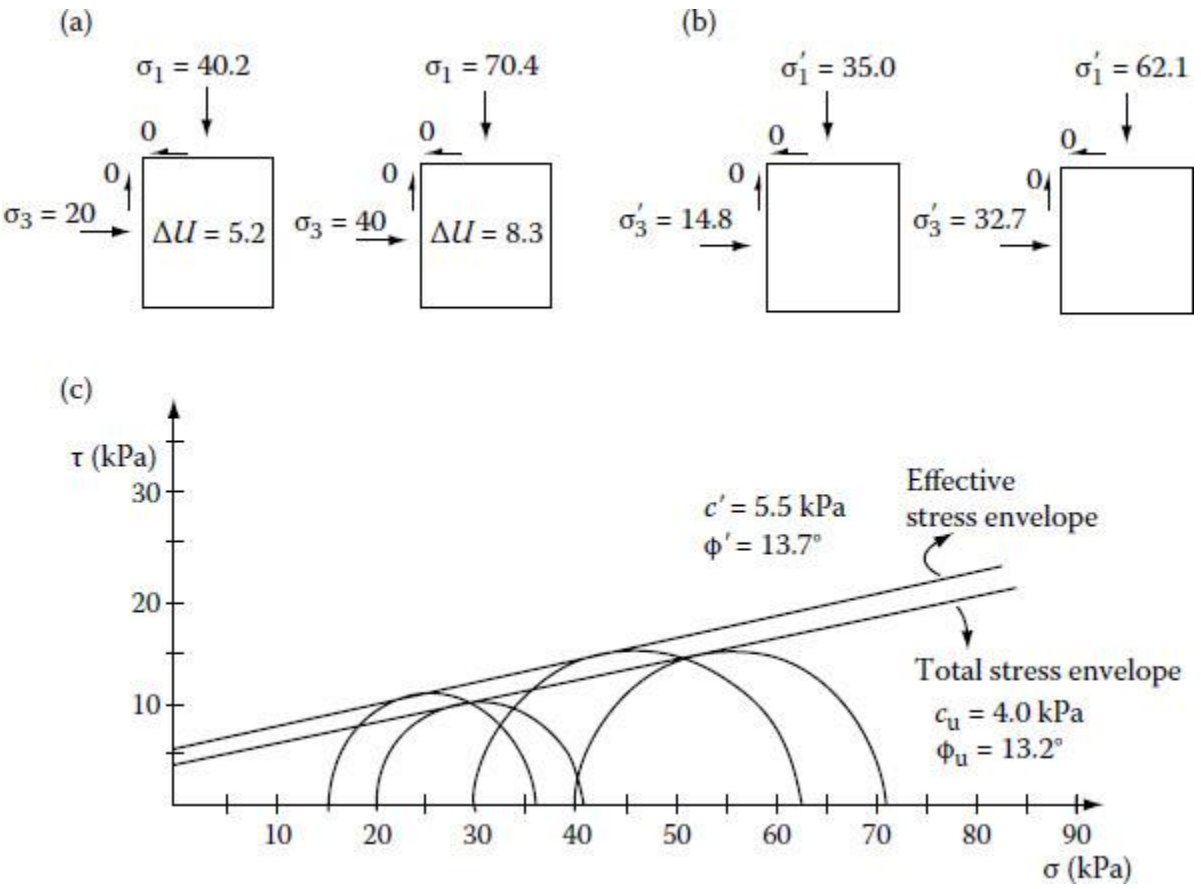

FIGURE 1.10

Stress states at failure for Example 1.2. (a) Total stress (kPa). (b) Effective stress (kPa). (From Edward Nawy (ed.), *Concrete Design Handbook*, Taylor & Francis, Boca Raton, FL, 1997.) (c) Mohr circle diagram for a CU test in Example 1.2. (From Edward Nawy (ed.), *Concrete Design Handbook*, Taylor & Francis, Boca Raton, FL, 1997.)

Effective Strength Parameters. The effective stresses on both (saturated) test samples at failure are computed by subtracting the pore pressure from the total stress (Equation 1.4a), as indicated in Figure 1.9b. The Mohr circles corresponding to the two stress states are drawn in Figure 1.10. The effective strength parameters (also referred to as the drained strength parameters) can be found from the slope of the Coulomb envelope for effective stresses plotted on the Mohr circle diagram as

$$c' = 5.5\text{kPa} \quad \text{and} \quad \phi' = 13.7^\circ$$

The most appropriate applications of the *c'* and #' parameters are cases where foundations are constructed rather slowly on well consolidated ground.

Example 1.3

Assume that one wishes to determine the strength properties of a medium stiff clayey foundation under short-term (undrained) conditions. The most effective method for achieving this is to conduct a UU (Quick) test. For the results presented in Table 1.3, estimate the undrained strength parameters.

Solution

In these tests, because the pore pressure generation is not typically monitored, the total stresses must be plotted, as in Figure 1.11. In Table 1.3, it can be seen that the deviator stress at failure does not change with the changing cell pressure during UU tests. This is because, in UU tests, since no drainage is permitted the soil samples are not consolidated to the corresponding cell pressures.

Therefore, the soil structure is largely unaffected by the change in cell pressure. Hence, the following strength parameters can be obtained from Figure 1.11:

$$C_u = 50.6\text{kPa} \quad \text{and} \quad \phi_u = 0^\circ$$

TABLE 1.3

Measured UU Triaxial Test Data

Test	Cell Pressure (kPa)	Deviator Stress at Failure (kPa)	Pore Pressure at Failure (kPa)
1	40	102.2	N/A
2	60	101.4	N/A

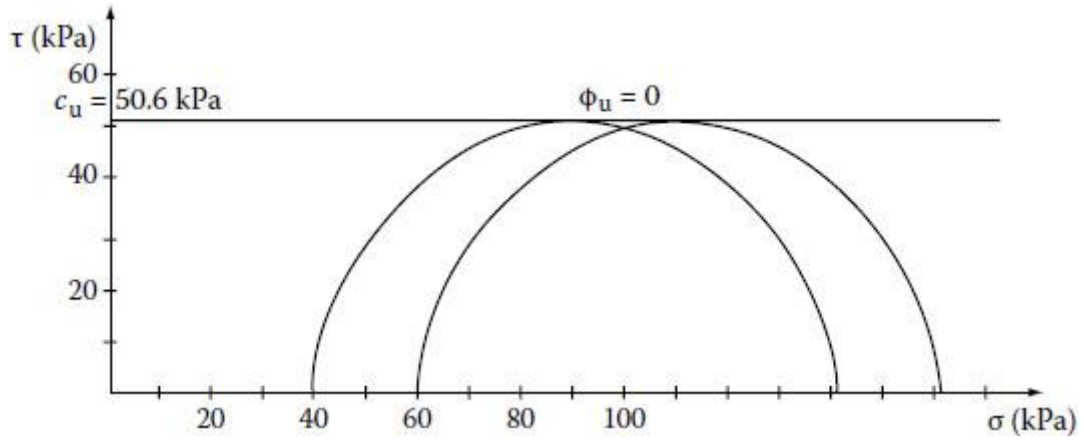

FIGURE 1.11

Mohr circle diagram for a UU test for Example 1.3. (From Edward Nawy (ed.), *Concrete Design Handbook*, Taylor & Francis, Boca Raton, FL, 1997.)

It is noted that the subscript "u" is used to distinguish the UU test parameters, and under UU conditions, if Equation 1.6 is applied, then the undrained shear strength $\tau_{f/u} = c_u$.

The most critical foundation design scenario presented by saturated, slow draining soils such as clays and silts involve undrained conditions prevailing immediately after the foundation is constructed. Therefore, the undrained shear strength (s_u) is typically used to design foundations on soils where the predominant soil type is clay or silt.

1.4.3 Unconfined Compression Test

Very often it is convenient to use the unconfined compression strength to express the undrained shear strength of clayey soils especially when *in situ* tests are used for such determinations. An unconfined compression test can be used to determine the C_u values based on the measured unconfined compression strength (q_u). Because this test can be visualized as an undrained triaxial test with no confining pressure (hence, unconsolidated), the Mohr circle for stress conditions at sample failure can be shown (Figure 1.12) as

$$c_u = \tfrac{1}{2} q_u \tag{1.11}$$

The same triaxial apparatus including the loading frame shown in Figure 1.8 can be used to test a clayey soil sample under unconfined compression conditions as well.

Example 1.4

Determine the unconfined compression strength and the undrained shear strength of the soil tested in unconfined compression conditions as shown in Table 1.4.

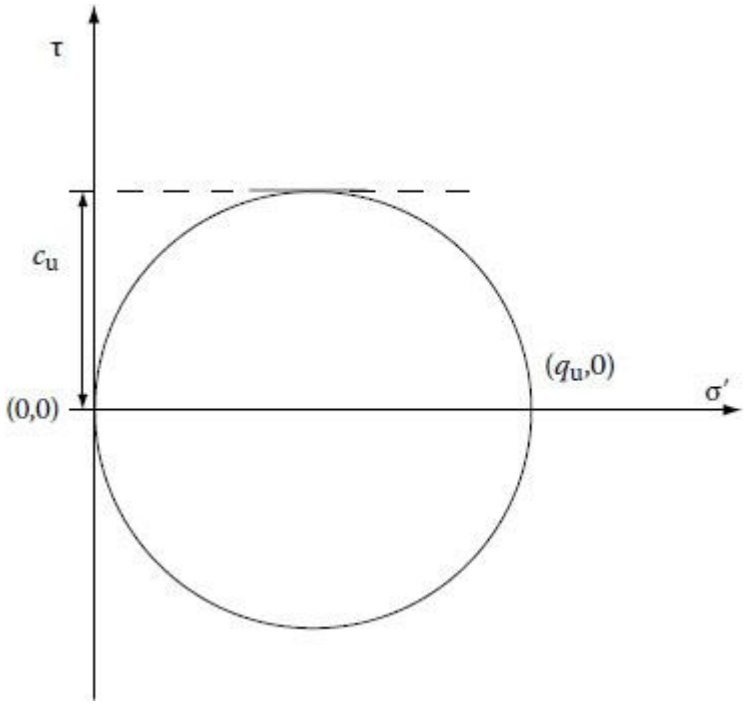

FIGURE 1.12
Mohr circle plot for failure stress condition in unconfined compression test.

TABLE 1.4
Data for Example 1.4

Vertical Displacement (mm)	Axial Force (N)	Strain (%)	Stress (kPa)
0.030	23.478	0.04	22.68
0.315	52.174	0.39	50.22
0.757	71.739	0.95	68.66
1.219	90.000	1.52	85.64
1.666	106.957	2.08	101.20
2.179	127.826	2.72	120.15
2.682	143.478	3.35	133.99
3.152	163.043	3.94	151.34
3.612	211.304	4.51	194.96
4.171	240.000	5.21	219.82
4.740	260.870	5.92	237.14
5.291	280.435	6.61	253.06
5.850	300.000	7.31	268.69
6.340	314.348	7.92	279.68

7.224	358.696	9.03	315.30
7.991	365.217	9.99	317.65
8.623	349.565	10.78	301.37
9.360	290.870	11.70	248.18

Note: Height of sample = 8 cm, initial cross-sectional area of sample = 10.35 cm^2.

It must be noted that the cross-sectional area modified for each testing stage has been used in computing the stress based on the following simple relationship that assumes the sample to be of constant volume throughout the test.

$$A_1 = A_0/(1-\varepsilon)$$

Solution

The compression test data in Table 1.4 are plotted in Figure 1.13. In Figure 1.13, the uncon-fined compression strength is determined to be 320 kPa. Therefore, from Equation 1.11, the undrained strength of the clay is estimated to be 160 kPa.

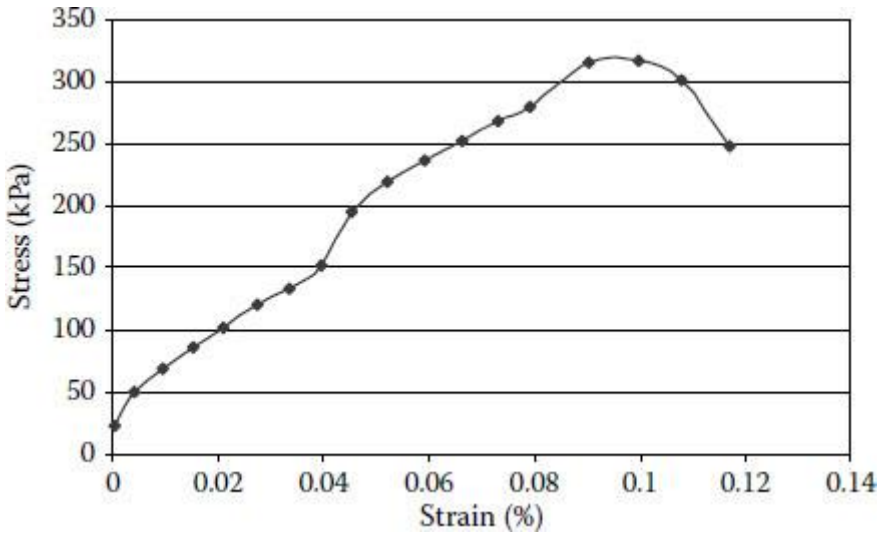

FIGURE 1.13

Plot of unconfined compression test results in Example 1.4.

1.5 Compressibility and Settlement

Soils, like any other material, deform under loads. Hence, even if the conditions needed for the structural integrity or adequate ground bearing of a foundation is satisfied, the ground supporting the structure can experience compressive deformations, leading to structural settlement. In most dry soils, this settlement will cease almost immediately after loading once soil particles readjust in order to attain equilibrium with the structural load. For convenience, this immediate settlement is evaluated using the theory of elasticity although it is quite often nonelastic in nature. However, if the ground material consists of wet, fine grained (low permeability) soil, the settlement will continue for a long period with slow drainage of water accompanied by readjustment of the soil skeleton until the excess pore water pressure dissipates completely. This phenomenon, known as

the primary consolidation, is usually evaluated by Terzaghi's consolidation theory. In some situations involving very fine clays and organic soils, settlement continues to occur even after the pore water pressure in the foundation vicinity comes to equilibrium with that of the far field. Secondary compression concepts introduced later in this chapter are needed to estimate this prolonged settlement. It is well known that primary consolidation and secondary compression cannot be separated on a time scale as the latter can occur even during dissipation of excess pore pressure.

1.5.1 Estimation of Immediate Settlement in Soils

The most commonly adopted analytical methods for immediate settlement evaluation in soils are based on the elastic theory. However, one must realize that reliable estimates of elastic moduli and Poisson ratio values for soils are not easily obtained. This is mainly because of the sampling difficulty and, particularly, the dependency of the elastic modulus on the stress state. On the other hand, reliable field methods for obtaining elastic moduli are also scarce. Very often, settlement of footings founded on granular soils or unsaturated clays is determined based on plate load tests (Chapter 4). The following expressions can be used to determine the immediate settlement:

$$s_e = f\frac{Bq_0}{E_s}(1-\upsilon_s^2)\frac{\alpha}{2}, \tag{1.12}$$

where

α = a factor to be determined from Figure 1.14

B = width of the foundation

L = length of the foundation

q_o = contact pressure (P/BL)

s_e = immediate settlement

E_s = elastic modulus of soil

υ_s = Poisson ratio of soil

f = 0.5 or 1.0 (depending on whether s_e is evaluated at the corner or center of the foundation)

Another widely used method for computing granular soil settlements is the Schmertmann and Hartman (1978) method based on the elastic theory as well.

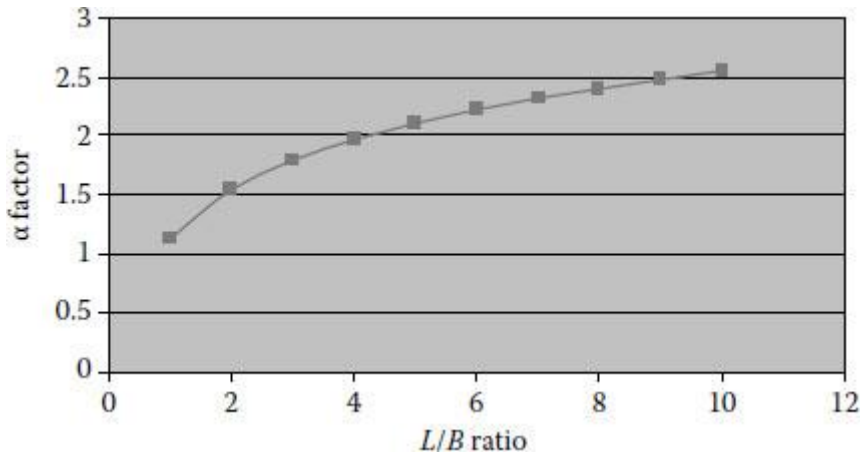

FIGURE 1.14

Chart for obtaining α factor. (Courtesy of B.M. Das. With permission.)

$$S_{\in} = C_1 C_2 (\Delta\sigma - q) \sum_{0}^{2B} \frac{I_z}{E_s} \Delta z \tag{1.13}$$

where

I_z = strain influence factor applicable for square or circular footing (Figure 1.15) (Schmertmann and Hartman, 1978)

C_1 = foundation depth correction factor = 1 - 0.5[q/Δσ − q)]

C_2 = correction factor for creep of soil = 1 + 0.2 log (time in years/0.1)

Δσ = stress at foundation level = P/BL

q = overburden stress at the foundation level (=γz)

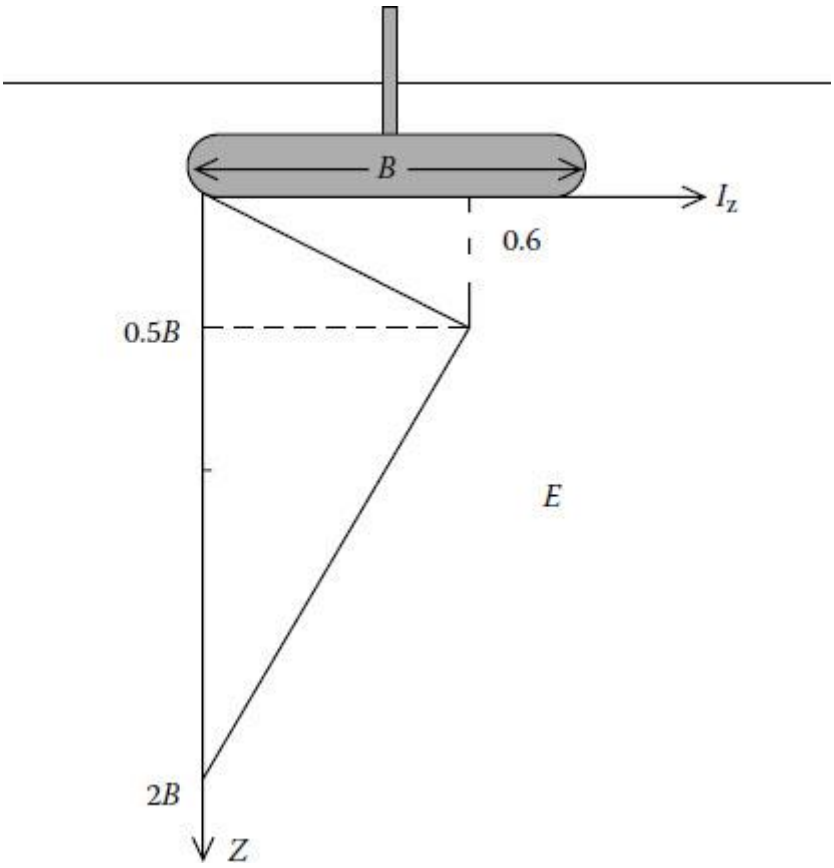

FIGURE 1.15

Strain influence factor.

TABLE 1.5

Poisson Ratios (v_s) for Geomaterials

Type of soil	v_s
Clay, saturated	0.4–0.5
Clay, unsaturated	0.1–0.3
Sandy clay	0.2–0.3
Silt	0.3–0.35

Sand, gravelly sand	−0.1 to 1.00
Commonly used	0.3–0.4
Rock	0.1–0.4 (depends somewhat on type of rock)
Loess	0.1–0.3
Ice	0.36
Concrete	0.15
Steel	0.33

Source: Bowles, J.E., *Foundation Analysis and Design*, McGraw-Hill, New York, 2002. With permission.

TABLE 1.6

Approximate Elastic Moduli of Geomaterials

Soil Type	**Elastic Modulus (MPa)**
Soft clay	2–25
Medium clay	15–50
Stiff clay	50–100
Loose sand	10–20
Medium dense sand	20–50
Dense sand	50–80
Loose gravel (sandy)	50–150
Dense gravel (sandy)	100–200
Silt	2–20

The elastic properties needed to manipulate the above expressions are provided in Tables 1.5 (Bowles, 2002) and 1.6, where the author, based on his experience, has extracted approximate values from Bowles (2002) for most common soil types. The following modifications to Figure 1.15 must be noted:

1. It is also common to use a strain influence plot consisting of two lines as shown in Figure 1.15 but with a different starting point (0,0.1) and a peak (0.5B,0,5). Inspection of the two alternatives will reveal that the areas under both of them would be equal.
2. When dealing with a strip footing, the coordinates of the peak and the bottom extreme must be changed to (B,0.7) and (4B,0), respectively.

1.5.1.1 Elastic Properties and In Situ *Test Parameters*

The most commonly used *in situ* tests that can be used to determine elastic properties of soil are the SPT and CPT tests discussed in Chapter 2. Some useful relationships that can provide the elastic properties from *in situ* test results are given in Table 1.7. However, in foundation engineering, it is also common to assume the following approximate relationships for granular soils.

$$E_s(\text{tsf}) = 8N \tag{1.14a}$$

$$E_s(\text{kPa}) = 768N, \tag{1.14b}$$

where N denotes the SPT blow count, and

$$E_s = 2q_c, \tag{1.15}$$

where q_c is the cone resistance in CPT measured in units of stress, and E_s and q_c have the same units.

A comprehensive example illustrating the use of the above relations is provided in Chapter 3 (Section 3.3).

TABLE 1.7

Soil Elastic Moduli from *In Situ* Test Data

Soil	SPT	CPT
Sand (normally consolidated)	$E_s = 500(N + 15)$ $= 7000\sqrt{N}$ $= 6000$ N	$E_s = (2 - 4)q_u$ [a] $= 8000\sqrt{q_c}$
Sand (saturated)	[b] E_s = (15,000-22,000) ln N $E_s = 250(N + 15)$	$E_s = 1.2(3D_r^2 + 2)q_c$ $E_s = (1 + D_r^2)q_c$ $E_s = Fq_c$ $e = 1.0, F = 3.5$ $e = 0.6, F = 7.0$
Sands, all (normally consolidated) Sand (overconsolidated)	$c_s = (2600 - 2900)$N [d] $E_s = 40,000 + 1050$N $E_{s(OCR)} = E_{s,nc}\sqrt{OCR}$	Es = (6–30)q_c [c]
Gravelly sand	E_s = 1200(N + 6) = 600(N + 6) $N \le$ [d] 15 = 600 (N + 6) + 2000 N > 15	
Clayey sand Silts, sandy silt, or clayey silt	$E_s = 320(N + 15)$ $E_s = 300(N + 6)$ If $q_c < 2500kPa$ use $E_s^r = 2.5q_c$ $2500 < q_c < 5000$ use $E_s^t = 4qc + 5000$ where E_s^t = constrained modulus = $\frac{E_3(1-\mu)}{(1+\mu)(1-2\mu)} = \frac{1}{m_\mu}$	Es = (3–6)qc Es = (1–2)qc
Soft clay or clayey silt		Es = (3–8)qc

Source: Bowles, J.E., *Foundation Analysis and Design*, McGraw-Hill, New York, 2002. With permission. *Note:* E_s in kPa for SPT and units of q_c for CPT; divide kPa by 50 to obtain ksf. The N values should be estimated as N_{55} and not N_{70}.

[a] E_s (elastic modulus) for SPT (standard penetration test) and units q_c for CPT (cone penetration test).

[b] USSR (may not be standard blow count N).

[c] Japanese Design Standard.

[d] Equation derived by Bowles, J.E. from plot of D'Appolonia et al. (1970).

1.5.2 Estimation of Foundation Settlement in Saturated Clays

When a foundation load is applied on a saturated fine-grained soil, it is immediately acquired by the pore water, as illustrated in Figure 1.16a. However, with the dissipation of pore pressure due to drainage of water, the applied stress (total stress) is gradually transferred to the soil skeleton as an effective stress (Figure 1.16b). The long-term rearrangement of the soil skeleton and the consequent foundation settlement that take place during this process is termed consolidation settlement.

The soil properties required for estimation of the magnitude and rate of consolidation settlement can be obtained from the laboratory one-dimensional (1-D) consolidation test. Figure 1.17 shows the consolidometer apparatus where a saturated sample (typically 2.5 in or 62.5 mm diameter and 1.0 in or 25.0 mm in height) is subjected to a constant load, whereas the deformation and (sometimes) the pore pressure are monitored until the primary consolidation process is complete. The resulting deformation is known as the "ultimate primary settlement." A detailed description of this test can be found in the work of Das (2002). The sample is tested in this manner for a wide range of stresses that encompasses the expected average pressure increase produced by the foundation in the clay layer.

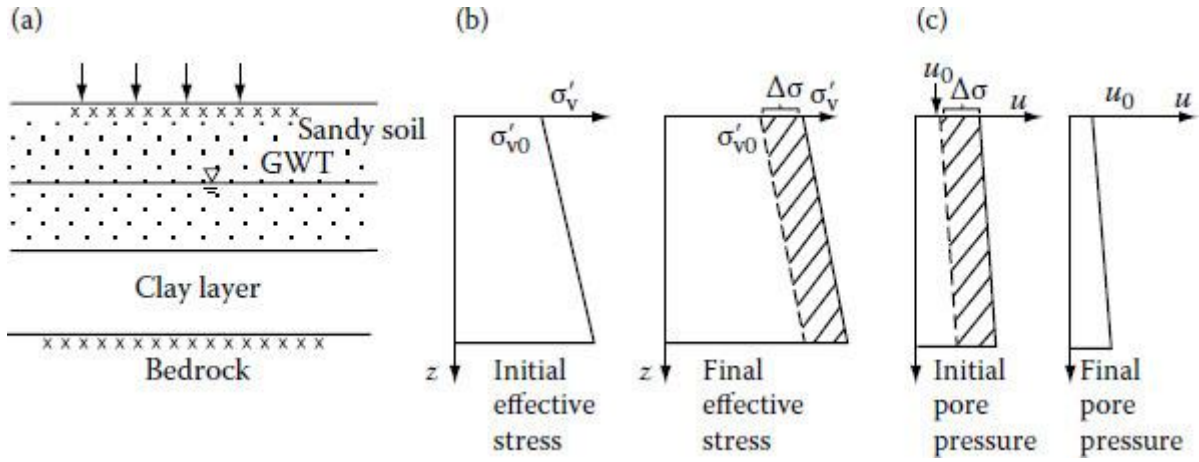

FIGURE 1.16

Illustration of consolidation settlement. (a) Subsurface profile. (b) Effective stress distribution. (c) Pore pressure distribution. (From Edward Nawy (ed.), *Concrete Design Handbook*, Taylor & Francis, Boca Raton, FL, 1997.)

FIGURE 1.17
Laboratory consolidometer apparatus. (Courtesy of the University of South Florida.)

Figure 1.18 shows the results of a consolidation test conducted on a clay sample. The coefficient of consolidation (C_v) for the soil can be obtained from the above results using the Casagrande logarithm-of-time method (Holtz and Kovacs, 1981). The coefficient of consolidation, C_v, is defined based on Equation 1.16.

$$T = \frac{C_v}{H_{dr}^2} \tag{1.16}$$

where H_{dr} is the longest drainage path in the consolidating soil layer and T is the nondimensional time factor corresponding to a time of t. It should be noted that water is permitted to drain from both sides of the laboratory soil sample during consolidation. Hence, H_{dr} = 0.5 in or 12.5 mm.

Furthermore, for a clay layer subjected to a constant or linear pressure increment throughout its depth, the relationship between the average degree of consolidation U (settlement at any time t as a percentage of the ultimate primary settlement) and the nondimensional time factor, T, shown in Table 1.8, can be derived using Terzaghi's 1-D consolidation theory.

Example 1.5

Compute the value of C_v using Figure 1.18.

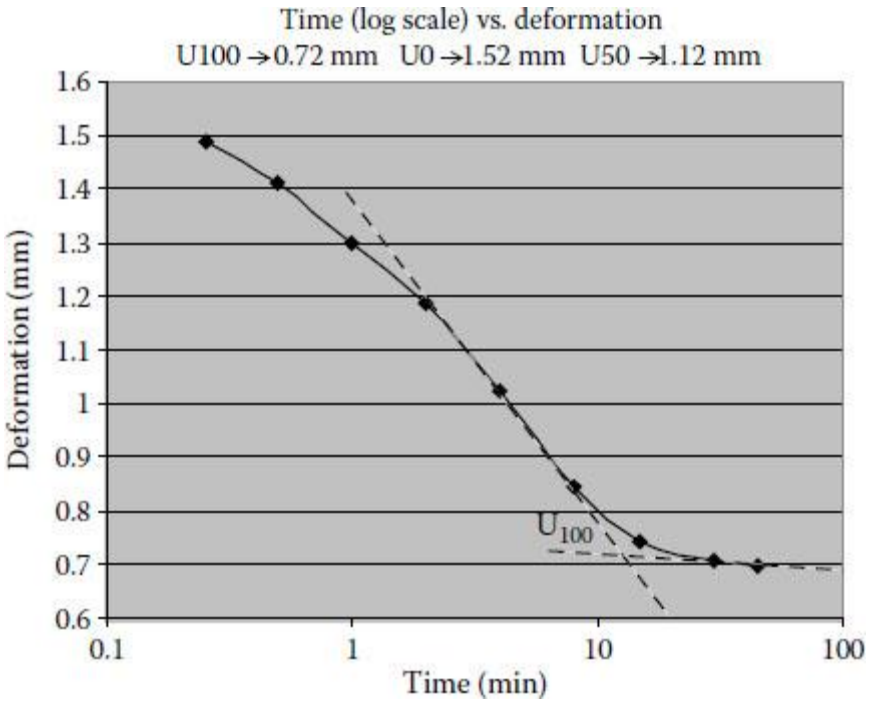

FIGURE 1.18
Settlement versus logarithm-of-time curve.

TABLE 1.8
Degree of Consolidation versus Time Factor

U_{avg}	T
0.1	0.008
0.2	0.031
0.3	0.071
0.4	0.126
0.5	0.197
0.6	0.287
0.7	0.403
0.8	0.567
0.9	0.848
0.95	1.163
1.0	∞

Solution

In Figure 1.18, when $U = 50\%$, $t = 135$ s
However, from Table 1.8, when $U = 50\%$, $T = 0.197$
Noting from above that $H_{dr} = 12.5$ mm
Substituting in Equation 1.16, $C_v = 0.228$ mm^2/s

When the above consolidation test is repeated for several different pressure increments, each time doubling the pressure, the variation of the post-consolidation (equilibrium) void ratio (e) with pressure (p) can be plotted using the following relations:

$$\frac{\Delta e}{1+e_0} = \frac{\Delta H}{H} \tag{1.17a}$$

$$e = e_0 - \Delta e \tag{1.17b}$$

where e_0 and H are the initial void ratio and the sample height respectively, whereas ΔH and Δe are their respective changes. It must be noted that when the primary consolidation due to an applied pressure of p is complete with dissipation of pore pressure and the equilibrium void ratio is reached, the effective stress in the soil (p') is equal to p. Hence, when e values corresponding to the applied pressure p are plotted, it is realized that in effect, the resulting plot is an e-versus-p' plot. A typical laboratory consolidation curve (e vs. log p') for a clayey soil sample is shown in Figure 1.19. The following important parameters can be obtained from Figure 1.19:

Recompression index, C_r = (1.095 – 1.045)/(log 60 – log 10) = 0.064
Compression index, C_c = (1.045 – 0.93)/(log 120 – log 60) = 0.382
Preconsolidation pressure, p_c = 60 kPa

All the above information can be used to estimate the ultimate consolidation settlement of a saturated clay layer (of thickness H) due to an average pressure increase in Δp. The ultimate consolidation settlement (s_{con}) can be determined by the following expressions,

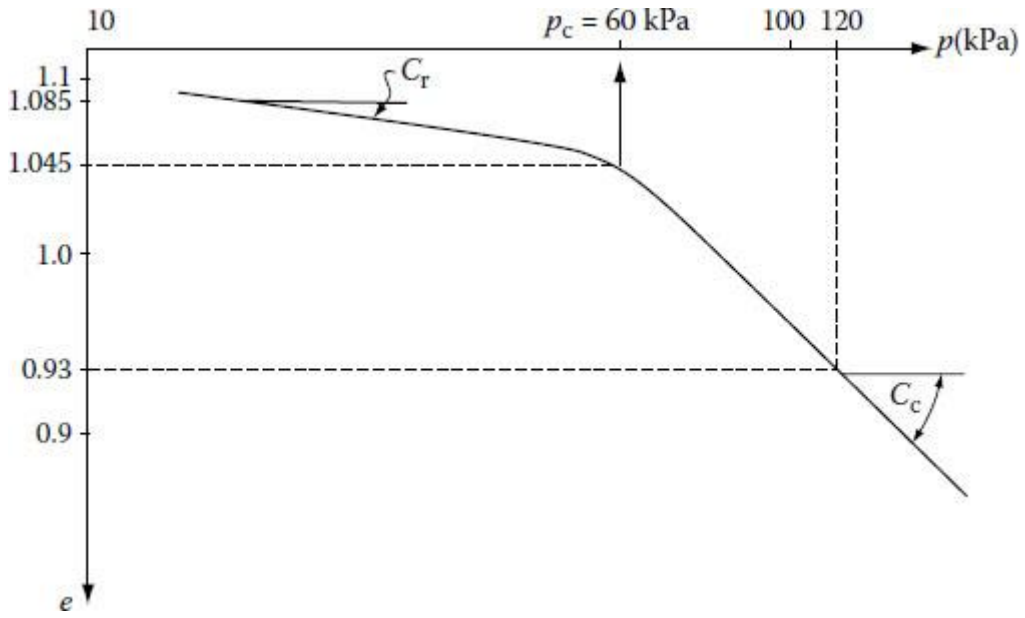

FIGURE 1.19

Laboratory consolidation curve (e vs. log p). (From Edward Nawy (ed.), *Concrete Design Handbook*, Taylor & Francis, Boca Raton, FL, 1997.)

depending on the initial stress state (σ'_{v0}) and the load increment $\Delta\rho$, as illustrated in Figure 1.20.

$$s_{ult} = \frac{C_c or C_r}{1+e_0} H \log\left(1 + \frac{\Delta p}{\sigma'_{v0}}\right)$$

Case $(\sigma'_{v0} > p_c)$

$$s_{con} = \frac{C_c H}{1+e_0} \log \frac{\sigma'_{v0} + \Delta p}{\sigma'_{v0}} \tag{1.18a}$$

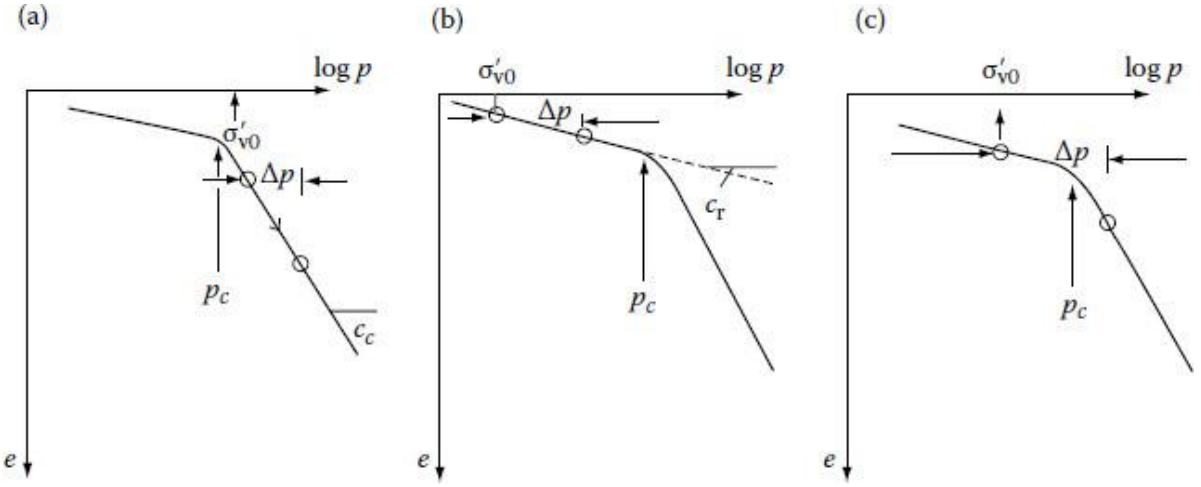

FIGURE 1.20
Illustration of the use of consolidation equation: (a) case 1, (b) case 2, and (c) case 3. (From Edward Nawy (ed.), *Concrete Design Handbook*, Taylor & Francis, Boca Raton, FL, 1997.)

Case $(\sigma'_{v0} + \Delta p < p_c)$

$$s_{con} = \frac{C_r H}{1+e_0} \log \frac{\sigma'_{v0} + \Delta p}{\sigma'_{v0}} \tag{1.18b}$$

Case $(\sigma'_{v0} + \Delta p > p_c > \sigma'_{v0})$

$$s_{con} = \frac{C_r H}{1+e_0} \log \frac{p_c}{\sigma'_{v0}} + \frac{C_c H}{1+e_0} \log \frac{\sigma'_{v0} + \Delta p}{p_c} \tag{1.18c}$$

Equations 1.18a through 1.18c can be derived easily based on Equation 1.17a and Figure 1.20.

The average pressure increase in the clay layer due to the foundation can be accurately determined by using Newmark's chart, shown in Figure 1.21. When the footing is drawn on the chart to a scale of $AB = d_c$, the depth of the midplane of the clay layer from the bottom of footing, Δp can be evaluated by Equation 1.19. The footing must be drawn so that the vertical projection of the location where the settlement is desired coincides with the center of the chart.

$$\Delta p = qIM, \tag{1.19}$$

where q, I, and M are the contact pressure, the influence factor (specific to the chart), and when the scaled footing is drawn on the chart, the number of elements of the chart covered by the drawn footing, respectively.

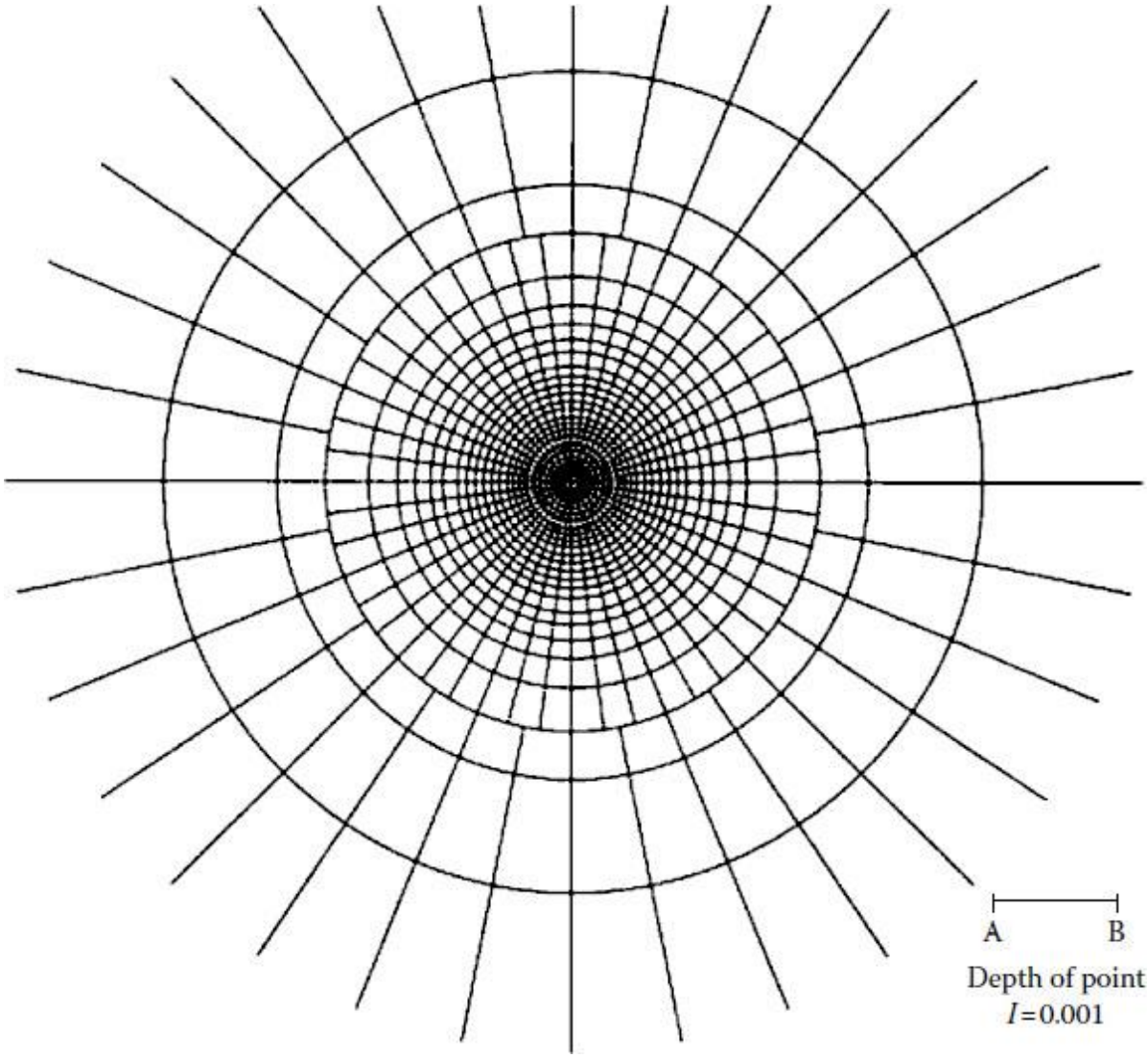

FIGURE 1.21
Newmark's chart.

1.6 Soil Densities and Compaction

It is essential for designers of foundations and retaining structures to possess a knowledge of the density of soils under different moisture states. In addition, a sound knowledge of how to determine and improve soil unit weights (densities) is vital. For this purpose, commonly used soil unit weights (densities) and the corresponding density, water content, and void ratio relations are introduced in the following sections.

1.6.1 Bulk Unit Weight

The *bulk or moist unit weight* (γ_b) is the total weight (W_T) of a unit volume of soil that includes water and air. In order to determine γ_b, one has to accurately estimate the volume (V_T) of a soil mass (Equation 1.20a). Hence, the estimation of *in situ* γ_b becomes somewhat of a difficult task addressed by specially designed tests such as the sand cone test (Section 1.6.6.2).

$$\gamma_b = \left(\frac{W_T}{V_T}\right) \tag{1.20a}$$

Typically, unit weights are expressed in kN/m^3 or lbf/ft^3.

On the other hand, using basic quantification properties of soil (such as the moisture content and the void ratio), the *bulk unit weight* of a soil can also be expressed conveniently as

$$\gamma_b = \gamma_w G_s\left(\frac{1+w}{1+e}\right) \tag{1.20b}$$

where

w = moisture content

e = voids ratio

G_s = specific gravity of solids that typically ranges between 2.5 and 2.75

γ_w = unit weight of water (9.8 kN/m^3 or 62.4 lbf/ft^3)

1.6.2 Dry Unit Weight

The dry unit weight (γ_d) is the weight of solids (W_s) of a unit volume of soil that includes water and air (Equation 1.21a).

$$\gamma_d = \left(\frac{W_s}{V_T}\right) \tag{1.21a}$$

Since the dry weight in Equation 1.21a does not include water.

Since the dry weight in Equation 1.21a does not include water, by setting the water content in Equation 1.20b to zero, it can be seen that the *dry unit weight* of a soil can be expressed conveniently as

$$\gamma_d = \gamma_w G_s\left(\frac{1}{1+e}\right) \tag{1.21b}$$

Then, using Equations 1.20b and 1.21b, one can derive the relationship (Equation 1.22) that allows the *dry unit weight* of a soil to be determined conveniently from the bulk unit weight.

$$\gamma_d = \left(\frac{\gamma_b}{1+w}\right) \tag{1.22}$$

1.6.3 Saturated Unit Weight

The relationship between the basic quantification properties of soil (Equation 1.23) fur nishes a valuable computational tool in unit weight estimations.

$$se = wG_s \tag{1.23}$$

where s = degree of saturation

Subsurface soil beneath the groundwater table or within the capillary zone is saturated with water. The bulk unit weight under saturated conditions is conveniently expressed by the *saturated unit weight* (γ_{sat}), which implies a *degree of saturation* (s) of 100%. Then, using an s value of 100%, one can use Equations 1.20b and 1.23 to express the *saturated unit weight* as

$$\gamma_{sat} = \gamma_w\left(\frac{G_s+w}{1+wG_s}\right) \tag{1.24}$$

1.6.4 Submerged (Buoyant) Unit Weight

In foundation stress computations (Equation 1.4b) involving "underwater" soil conditions, the buoyant effect due to the water table can be included directly by using the *submerged or buoyant unit weight γ'* (Equation 1.25), in place of the *saturated unit weight.* This is especially useful in effective stress computations because the need for separate consideration of pore pressure (Equation 1.4b) can be precluded.

$$\gamma' = \gamma_{sat} - \gamma_w \tag{1.25}$$

1.6.5 Relative Density

The degree of packing of discrete particles in granular soils such as sand and gravel can be expressed using the relative density parameter defined as follows:

$$D_r = \left[\frac{(e-e_{min})}{(e_{max}-e_{min})}\right] \times 100\%, \tag{1.26}$$

where

e = void ratio in the natural state of the soil

e_{min} = minimum attainable void ratio under maximum compaction (practically achieved with vigorous vibration)

e_{max} = maximum attainable void ratio under minimum compaction (practically achieved with fluviation in air or water)

From Equation 1.26, it is noted that $D_r = 0$ for the loosest condition ($e = e_{max}$) and $D_r = 100\%$ for the densest condition ($e = e_{min}$).

1.6.6 Soil Compaction

Before construction of building foundations, newly constructed embankments and natural subgrades must be compacted to density specifications within the limitations of water content. One has to generally perform a laboratory compaction test on the foundation soil in advance, in order to set the appropriate field compaction specifications. The two commonly performed tests are (1) standard Proctor compaction test and (2) modified Proctor compaction test. This section provides a summary of the laboratory compaction computations. The reader is referred to Das (2002) for experimental details of these tests.

1.6.6.1 Laboratory Compaction

During laboratory compaction tests, a sample from the foundation soil is compacted at different water contents using the standard compaction equipment shown in Figure 1.22. The weight of the compacted soil filling the standard mold, and its water content are recorded in each trial as shown in Table 1.9. Then, the laboratory compaction curve is plotted based on this data as indicated in Figure 1.23.

FIGURE 1.22
Laboratory soil compaction equipment. (Courtesy of the University of South Florida.)

TABLE 1.9
Data for Example 1.6

Mass of Compacted soil and Mold (g)	Compacted Water Content (%)	Unit Weight (kN/m^3), equation 1.20a	Dry Unit Weight (kN/m^3), equation 1.22	Dry Unit Weight (kN/m^3) at 100% Saturation, equation 1.24/(1+w)
5873	4.48	17.383	16.637	23.214
6012	10.18	18.840	17.100	20.452
6001	15.99	18.722	16.142	18.241
6046	20.33	19.193	15.951	16.877

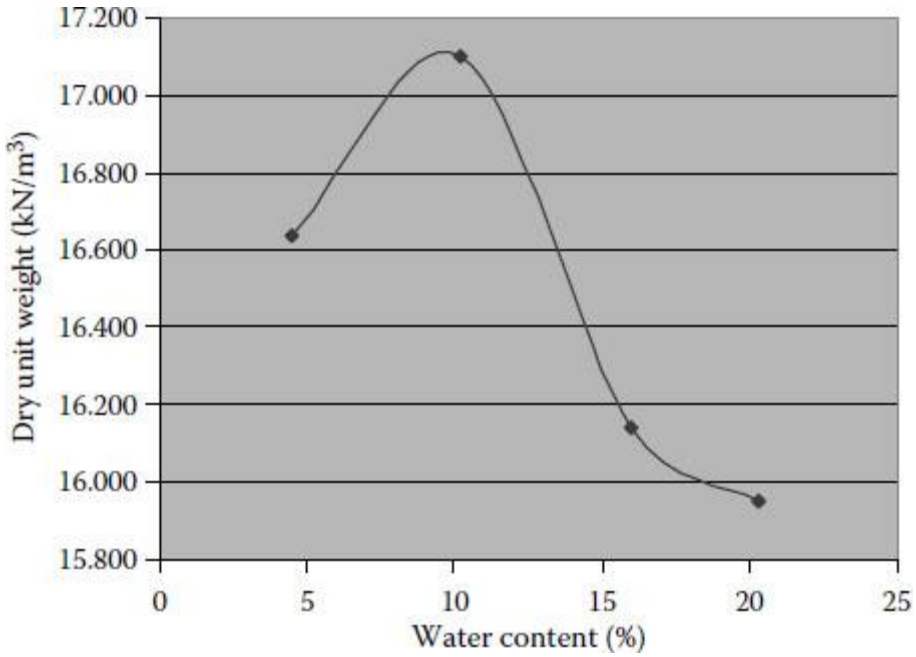

FIGURE 1.23
Laboratory compaction plot for Example 1.6.

Example 1.6

Plot the compaction curve for the data provided in the columns 2 and 4 of Table 1.9 for a standard Proctor compaction test, and determine the maximum dry unit weight achievable under standard compaction conditions and the corresponding optimum water content. Note that the mass and the volume of the standard compaction mold (Figure 1.22) are 4200 g and 940 mL, respectively.

Solution

Table 1.9 also shows the computational procedure used to obtain the *bulk unit weight* and the *dry unit weight* for each trial based on Equations 1.20a and 1.22. Figure 1.23 illustrates the plot of *dry unit weight* of the compacted soil versus the water content. It can be seen in Figure 1.23 that

(1) Maximum dry unit weight = 17.1 kN/m^3

(2) Optimum water content = 10%

It is also quite common to plot the 100% degree of saturation line on the same plot (Table 1.9, column 5). Based on the above laboratory results, the specifications for field compaction of the particular soil can be set as follows.

Compacted *dry unit weight* in the field must be at least 98% of the laboratory *maximum dry unit weight* (i.e., 17.1 kN/m^3). The field water content must be within 2% of the optimum water content found in the laboratory (i.e., between 8% and 12%).

1.6.6.2 Evaluation of Field Compaction

Unit weights of compacted *in situ* soils and newly laid embankments can be evaluated using many methods. The most common ones are (1) sand cone test, (2) rubber balloon test, and (3) the nuclear gauge method. Experimental details of the first two methods are found in the work of Holtz and Kovacs (1981), whereas use of the nuclear gage is described in detail by Wray (1986). In this chapter, a numerical example illustrating the sand cone test procedure is presented. The equipment used in the sand cone test is shown in Figure 1.24.

Example 1.7

Estimate the field dry unit weight of a given embankment fill based on the sand cone test readings provided below. For the benefit of the reader, the recorded data are italicized to differentiate them from the computations.

Solution

Step 1. Determination of density of sand in the laboratory

A uniformly graded sand (typically Ottawa sand) that is not very sensitive to compaction is used for the calibration. Hence, the density of this sand, which is assumed to be invariant, can be first established based on measurements made with a mold of a known volume (e.g., standard compaction mold of volume 940 mL).

Diameter of mold = 10.13 cm
Height of mold = 11.65 cm
Mass of mold and sand = 5602 g
Mass of empty mold = 4252 g
Volume of mold = 938.94 cm^3
Mass of sand in mold = 1350 g
Density of sand = 1.4378 g/cm^3 = 1437.8 kg/m^3

Step 2. Determination of mass of sand to fill cone

The next step is to determine the volume of the cone (Figure 1.24) by filling it with the calibrated sand (Ottawa sand)

FIGURE 1.24
Equipment for sand-cone test. (Courtesy of the University of South Florida.)

TABLE 1.10
Water Content for Example 1.7

	Trial 1	Trial 2	Trial 3
Mass of container + wet soil (g)	146.54	142.52	147.32
Mass of container + dry soil (g)	144.63	140.89	144.83

Mass of container (g)	113.65	104.89	104.18
Moisture content	6.16%	4.52%	6.13%

Mass of jar and cone before filling the cone = 3516 g
Mass of jar, cone, and sand after filling the cone = 1934 g
Mass of sand filling the cone = 1582 g

Step 3. In place measurements
Then, the sand-cone apparatus is placed on a previously dug hole in the (field) compacted soil, and Ottawa sand is poured in gently until it completely fills the hole. On the other hand, the *in situ* soil removed from the hole is collected into a pan and weighed. The volume of the hole created by the removal of soil is estimated by knowing the amount of calibrated sand required to fill the hole and the cone.

Mass of jar and sand before use = 6538 g
Mass of jar and sand after use = 4325 g
Mass of collected soil = 870 g
Mass of sand in hole + cone = 2213 g
Mass of sand in hole = 2213 - 1582 = 631g

Volume of sand in hole = 631 g/1.4378 (see Step 1) = 438.9 cm^3

From Equation 1.20a,

Bulk density of Soil = 870/438.9 = 1.9824 g/cm^3 = 1982.4 kg/m^3

Step 4. In-place moisture content measurements
Finally, a simple water content test is performed for the soil fill as indicated in Table 1.10.

Average moisture content = 1/3 (6.16% + 4.52% + 6.13%) = 5.6%

Based on Equation 1.22,

Dry density = 1982.4/1.056 = 1877 kg/m^3
Dry unit weight = $1877(9.8)/10^{-3}$ = 18.39 kN m^{-3}

1.7 Concepts of Unsaturated soil Mechanics

1.7.1 Effective Stresses

Although unsaturated subsurface soils are common in most building sites, the concepts of unsaturated soil mechanics are rarely introduced in geotechnical designs. Furthermore, most geotechnical engineering problems are solved assuming positive pore water pressures when suction can occur even in saturated soils due to capillarity. The solutions of many practical problems involving unsaturated soils require an understanding of the hydraulics, mechanics, and interfacial physics of unsaturated soils (Lu and Likos, 2004).

Soils are generally saturated below the groundwater table with positive water pressure, whereas a capillary fringe with negative pore water pressures (suction) occurs immediately above the water table where the degree of saturation approaches 100%. However, in close proximity to the ground surface the pore water pressure is reduced due to evaporation and evapotranspiration. Continued development of these conditions can induce suction (or tension) and eventual desaturation of the

superficial soils. In unsaturated soils, air and water coexist in the interconnected pore channels forming a three phase system. Although the air–water interface (contractile skin) should be considered as the fourth phase, it is neglected in most studies.

In wet unsaturated soils, the effective stress at a given location is expressed by a modi fied form of Equation 1.5 as

$$\sigma' = \sigma - u_a + \chi(u_a - u_w), \tag{1.27}$$

where

u_a = pressure of gas, vapor, or air
χ = parameter related to the degree of saturation (0 for dry oil and 1.0 for saturated soils)

The χ value applicable for a given degree of saturation must be determined by experimentally simulating the corresponding loading condition (volumetric deformation or shear deformation).

The term $(u_a - u_w)$ is denoted as matric suction, which is known to be one of the stress state variables controlling the mechanical behavior of unsaturated soils or any soil with negative pore water pressure such as collapsible soils, swelling soils, and residual soils. Methods of measuring matric suction in soils are important for predicting the deformation behavior of unsaturated soils. For more information on such methods, the reader is referred to Clifton et al. (1999) and Fredlund and Morgenstern (1977).

1.7.2 Soil Water Characteristic Curve and Water Moisture Retention Curve

The soil water characteristic curve (SWCC) depicts the relationship between volumetric soil water content (θ) and soil water pressure potential (suction, Ψ). The soil parameters defining a typical SWCC are shown in Figure 1.25a, whereas the SWCC for different soil types are presented in Figure 1.25b. Figure 1.25 shows that sands lose water quite readily upon suction-induced drainage, whereas silts and clays lose much less water upon drainage. There are a number of empirical equations proposed to best fit the SWCCs using the soil parameters shown in Figure 1.25.

$$\text{Volumetric water content, } \theta = \frac{V_w}{V}, \tag{1.28}$$

where V is the total volume of a soil sample and V_w is the volume of water.

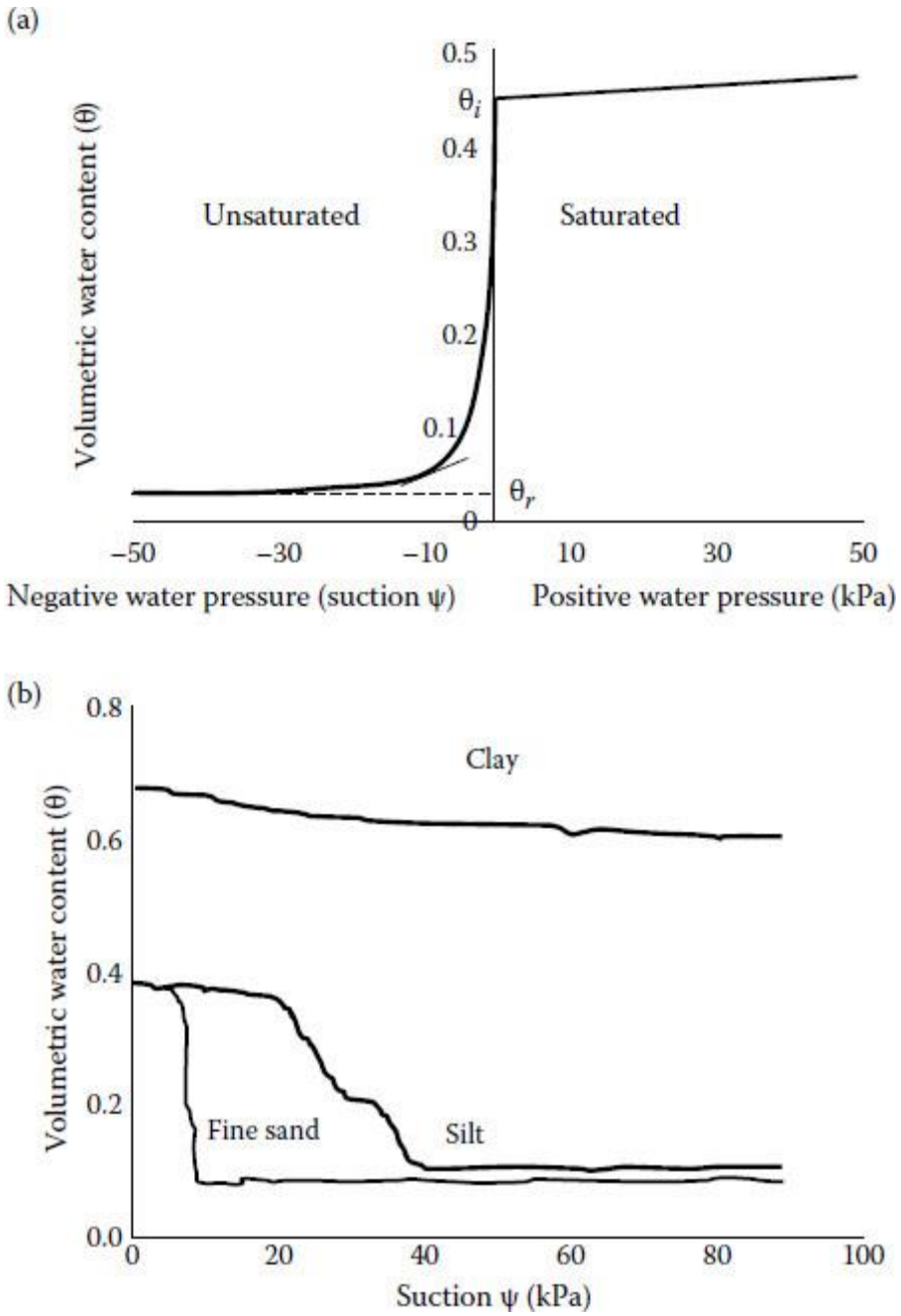

FIGURE 1.25

(a) Typical soil-water characteristic curve for a saturated-unsaturated soil. (b) Soil-water characteristic curve for specific soil types. (From Lam, L. et al., *Can Geotech J*, 24, 565–580, 1987.)

$$\theta = C(\psi)\frac{\theta_s}{\left\{\ln\left[e+\left(\frac{\psi}{a}\right)^n\right]\right\}^m}, \tag{1.29}$$

where *e* denotes the base of natural log = 2.718, C(ψ) is a correction function defined in Equation 1.30, B_s is the (saturated) volumetric water content at zero pressure, and a, m, and *n* are fitting parameters.

$$C(\psi) = \frac{-\ln(1+\psi/\psi_r)}{\ln\left[1+(10^6/\psi_r)\right]} + 1, \tag{1.30}$$

where ψ_r (in kPa) is the suction corresponding to the residual water content, θ_r.

TABLE 1.11
Parameters Used to Define SWCC for Sand

ψ_r	30 kPa
θ_s	0.45
a	1.948 kPa
m	1.084
n	2.708

Source: Lam, L. et al., *Can Geotech J*, 24, 565–580, 1987.

Using fundamental soil mechanics, the degree of saturation can be shown to be

$$s = \frac{\theta}{n}, \tag{1.31}$$

where s is the degree of saturation and n is the total porosity of the soil. The parameters used in Equations 1.29 and 1.30 relevant to the fine sands are shown in Table 1.11.

An example problem on effective stress on unsaturated soils is solved in Example 1.8 at the end of this chapter. In addition, water flow characteristics of unsaturated soils are briefly described in Chapter 13.

1.8 Numerical Methods Used in Modeling of Earthen Structures

1.8.1 Finite Difference Approach

The load deformation behavior of most geotechnical engineering problems can be modeled by ordinary or partial differential equations. In the majority of them, the independent variables are either temporal or spatial variables. Solutions to most problems involving dynamic or transient loading situations such as behavior of machine foundations and pile driving are primarily time- and space-dependent, whereas those of static loading problems are based on spatial variables only.

If the geometry of the problem and loading conditions is relatively uncomplicated, then conventional mathematical solutions can be derived for the above problems. In such cases, the constants of integration are evaluated using one of the following two methods:

1. Dynamic and transient loading situations with known initial deformation of the geotechnical structure. This category of problems is known as *initial value* problems.
2. Static loading conditions with fixed boundary loading and deformation conditions. This category of problems is known as *boundary value* problems.

It is also realized that some loading conditions give rise to combined initial and boundary value problems. If the geometry of the problem and loading conditions is complicated, it would be impractical to derive explicit solutions to the governing differential equations. In such cases, numerical solution techniques offer attractive alternatives. Numerical solution of ordinary or partial differential equations is based on replacing the respective direct or partial derivatives with their corresponding numerical difference forms. Therefore, the consequent solution is limited to temporal instants or spatial locations at convenient predefined finite intervals, which are used for the definition of the above derivatives. These instants or locations are known as *nodes*, whereas their

assembly is called a finite difference *mesh.* One realizes that the accuracy of the solution depends on the fineness of the mesh. However, with the advent of powerful computers and computational techniques, numerical solutions can be refined to achieve the exact solutions in many problems. Finite difference techniques are particularly attractive for situations where the loading and geometrical conditions are nonhomogeneous.

Numerous finite difference solutions are illustrated in this handbook in the solution of following problems:

1. Footings on elastic foundations—Chapter 4
2. Pile driving analysis—Chapter 9
3. Two-dimensional seepage—Chapter 13

1.8.2 Finite Element Approach

The finite element method (FEM) is widely used to model the load deformation behavior of foundations, piles, retaining walls, and other earthen structures, and perform important parametric studies relating to their design. With the availability of sophisticated and efficient computational facilities, finite element analysis can facilitate effective design criteria, even on a case-by-case basis, with the aid of parametric studies that involve design parameters relevant to each case. It is particularly attractive for situations involving the design of irregular and relatively complex earthen structures. The basic philosophy involved in modeling an earthen structure with the FEM can be summarized by the following basic principles that form the framework of the FEM formulation:

1. Satisfy the force equilibrium of each finite soil or structural element.
2. Satisfy the deformation compatibility at nodal points of each finite element considered.
3. Incorporate an appropriate stress–strain behavior model for each soil or structural material that composes the structure.

The mathematical techniques used to achieve the above tasks will be summarized later in this chapter.

However, because of their very nature, finite element solutions also suffer from all draw backs characteristic of numerical approximations. Based on the above discussion, one realizes that the two most important steps that require special attention of the analyst are as follows:

1. Discretization of the soil/structure influence zone into finite soil or structural elements that could capture all of the load, deformation, geometric, and boundary effects that determine the overall behavior of the particular earthen structure under the given loading conditions.
2. Selection of the appropriate constitutive models that would describe, as accurately as possible, the stress–strain behavior of different soil and structural materials that make up the earthen structure being analyzed.

1.8.3 Finite Element Formulation

The first step involved in the formulation is the determination of the type of element to be used in modeling. Then the strain field at any point on the selected soil (or structural) element must be expressed in terms of the nodal deflections. Analysts have used a variety of different elements ranging from linear triangular elements, bilinear quadrilateral elements, trilinear hexahedral

elements, etc., depending on their applicability (Hughes, 1987) to modeling different loading situations. The use of isoparamatric quadrilateral elements has been common in geotechnical modeling because they can be designed to take on convenient shapes, such as curved boundaries, often encountered in geotechnical problems. Standard nodal shape functions (N) for many elements are available in the literature (Zienkiewicz et al., 1977; Hughes, 1987).

The significance of the nodal shape function of a quadrilateral element, N,, where j (j = 1–4) denotes the local node number, is that the coordinates, displacement, velocity, or the acceleration of any point within a given soil (or structural) element, can be expressed in terms of corresponding nodal values, using the shape functions as follows:

$$u_i(t) = \sum_{j=1}^{4} N_j(\xi,\eta) u_i^j(t). \tag{1.32}$$

where

N,(ξ, η) = shape function for the local node j in the local isoparametric coordinates (ξ, η).

$u_i^j(t)$ = time variation of any physical quantity i (coordinates, displacement, velocity or acceleration) of the nodal point j. $u_i(t)$ = time variation of the corresponding physical quantity i at any other point within the element.

An example of shape functions for isoparametric bilinear quadrilateral elements is pro vided below:

$$N_1(\xi, \eta) = \tfrac{1}{4}(1-\xi)(1-\eta) \tag{1.33a}$$

$$N_2(\xi,\eta) = \tfrac{1}{4}(1+\xi)(1-\eta) \tag{1.33b}$$

$$N_3(\xi, \eta) = \tfrac{1}{4}(1+\xi)(1+\eta) \tag{1.33c}$$

$$N_4(\xi,\eta) = \tfrac{1}{4}(1-\xi)(1+\eta) \tag{1.33d}$$

It is realized that if the analyst is only concerned with the static behavior of an earthen structure, then the time variation need not be considered and the modeling problem becomes far less complicated. In such cases, the quantity u will only represent the displacement of the points (or the nodes) of interest.

The strain field (ε) at any location can be expressed in terms of the differential form of the displacement field (u) of that point as

$$\bar{\varepsilon} = [\mathbf{B}]\bar{u} \tag{1.34}$$

The following are several examples of strain-displacement matrices [**B**].

For 2-D (plane stress or plane strain) situations involving two displacements in $\bar{u}$ (u and v) and three strains in $\bar{\varepsilon}(\varepsilon_{xy}\varepsilon_y, \gamma_{xy})$,

$$[B] = \begin{bmatrix} \frac{\partial}{\partial x} & 0 \\ 0 & \frac{\partial}{\partial y} \\ \frac{\partial}{\partial y} & \frac{\partial}{\partial x} \end{bmatrix} \tag{1.35}$$

For 3-D axisymmetric situations (e.g., axial loading of piles) that can be described by only two displacements in $\bar{u}$ and four strains in $\bar{\varepsilon}\left(\varepsilon_r, \varepsilon_z, \varepsilon_0, \gamma_r\right)$,

$$[B] = \begin{bmatrix} \frac{\partial}{\partial r} & 0 \\ 0 & \frac{\partial}{\partial z} \\ \frac{1}{r} & 0 \\ \frac{\partial}{\partial z} & \frac{\partial}{\partial r} \end{bmatrix} \tag{1.36}$$

Strain components can be related to the corresponding stresses using the constitutive relations matrix as follows:

$$\bar{\sigma} = [D]\bar{\varepsilon} \tag{1.37}$$

For 2-D (plane stress or plane strain) situations,

$$\bar{\sigma} = [\sigma_x \quad \sigma_y \quad \tau_{xy}]^T \tag{1.38}$$

For 3-D axisymmetric situations,

$$\bar{\sigma} = [\sigma_r \sigma_z \sigma_\theta \gamma_{xy}]^T \tag{1.20}$$

In the case of soil or structural elements that exhibit elastic behavior, the [**D**] matrix can be expressed for plane strain conditions as follows:

$$[D] = \frac{E}{(1+v)(1-2v)} \begin{bmatrix} 1-v & v & 0 \\ v & 1-v & 0 \\ 0 & 0 & (1-2v)/2 \end{bmatrix}, \tag{1.40}$$

where E and ν are the elastic modulus and the Poisson ratio of the element material, respectively. Similarly, the incremental form of Equation 1.37 can be used to model the nonlinear elastic behavior that is predominantly exhibited by soils at low stress levels as follows:

$$[\Delta\sigma]=[D][\Delta\varepsilon] \tag{1.41}$$

$$[D] = \frac{E}{(1+v_t)(1-2v_t)} \begin{bmatrix} 1-v_t & v_t & 0 \\ v_t & 1-v_t & 0 \\ 0 & 0 & (1-2v_t)/2 \end{bmatrix}, \tag{1.42}$$

where E_t and v_t are the respective instantaneous (tangential) elastic modulus and the Poisson ratio applicable to the current stress level, respectively.

However, it is the yielding of soils that governs the behavior of foundations in most loading cases (e.g., short piles subjected to lateral loading). Therefore, some soil constitutive relations that are commonly used to model the yielding (plastic) behavior of soil are discussed separately in Section 1.9.

By combining Equations 1.37 and 1.34, the stress vector can be expressed as

$$\bar{\sigma} = [\mathbf{D}][\mathbf{B}]\bar{u} \tag{1.43}$$

1.8.4 Equilibrium and Compatibility Conditions

When FEM is used to solve geomechanics problems involving static or dynamic conditions, one must satisfy the force equilibrium equations or the equations of motion, respectively. On the other hand, for any general system, the equations of motion must be satisfied under transient conditions. In addition, the volumetric compatibility between the pore water and the soil skeleton must be assured as well. Therefore, the equations of equilibrium (or motion) can be combined with those of volumetric compatibility between the pore water and the soil skeleton. As an example, in the case of axisymmetric problems, the resulting equation can be expressed for *any given point* in the radial (r) direction as (Zienkiwicz et al., 1977)

$$\frac{\partial \varepsilon_v}{\partial t} + \frac{\partial}{\partial r}\left[-\frac{k}{\gamma_w}\frac{\partial p}{\partial z} - \frac{k}{g}\ddot{u}\right] - \frac{\partial p}{\partial t}\frac{1-n}{K_s} + \frac{\partial \sigma_m}{\partial t}\frac{1}{K_s} + \frac{\partial p}{\partial t}\frac{n}{K_w} = 0, \tag{1.44}$$

where

u = displacement of a point in the r direction
e_v = average volumetric strain in the element
k = coefficient of hydraulic conductivity (permeability) assumed to be the same in all directions (isotropic condition)
p = pore water pressure
a_m = mean normal stress = $(\sigma_r + \sigma_z + \sigma_\theta)/3$
n = porosity of the soil skeleton = void ratio/(1 + void ratio) (Section 1.6)
K_s = compressibility of the solid grains
K_w = compressibility of water

Similar equations can be written in the other directions (i.e., z and θ) as well. Then, using the standard Galerkin method (Zienkiwicz et al., 1977), the above equation for a single point can be generalized for *an entire isoparametric finite element* in the following integral form:

$$\int_V [N]^T\left[\frac{\partial \varepsilon_r}{\partial t} + \frac{\partial}{\partial r}\left[-\frac{k}{\gamma_w}\frac{\partial p}{\partial z} - \frac{k}{8}\dot{u}\right] - \frac{\partial p}{\partial t}\frac{1-n}{K_s} + \frac{\partial \sigma_m}{\partial t}\frac{1}{K_s} + \frac{\partial p}{\partial t}\frac{n}{K_w}\right] = 0 \tag{1.45}$$

where

$$[N] = \begin{bmatrix} N_1 & 0 & N_2 & 0 & N_3 & 0 & N_4 & 0 \\ 0 & N_1 & 0 & N_2 & 0 & N_3 & 0 & N_4 \end{bmatrix}, \tag{1.46}$$

where N are defined by Equation 1.33 and V is the volume of the finite element.

Finally, by applying the standard FE procedure (Equations 1.33–1.43) and summing up Equation 1.45 over m number of elements covering the entire domain that is modeled, the following stiffness relationship can be derived (Zienkiwicz et al., 1977)

$$\sum_{n=1}^{m}\int_{V_n}(\rho[N]^T[N]\ddot{u})dV + \int_{V_n}([B]^T[D][B]u)dV + \int_{V_n}([N]^T[N]p)dV - \int_{b_n}([N]^T t)ds = 0, \tag{1.47}$$

where

V_n = volume of the nth finite element

b_n = boundary of nth finite element
t = traction (force per unit length) along the boundary of the nth element

It is also seen how Equations 1.34 and 1.37 have been used in substituting for [σ] in Equation 1.45.

Equation 1.47 is usually integrated within each element using the Gauss quadrature method. The integration points used in 2 × 2 Gauss quadrature technique are indicated in Figure 1.26. After the integration operation and mathematical manipulation, Equation 1.47 can be arranged in a format similar to Equation 1.48 and the corresponding stiffness matrix, [**K**], of the foundation structure can be obtained by comparison with Equation 1.48.

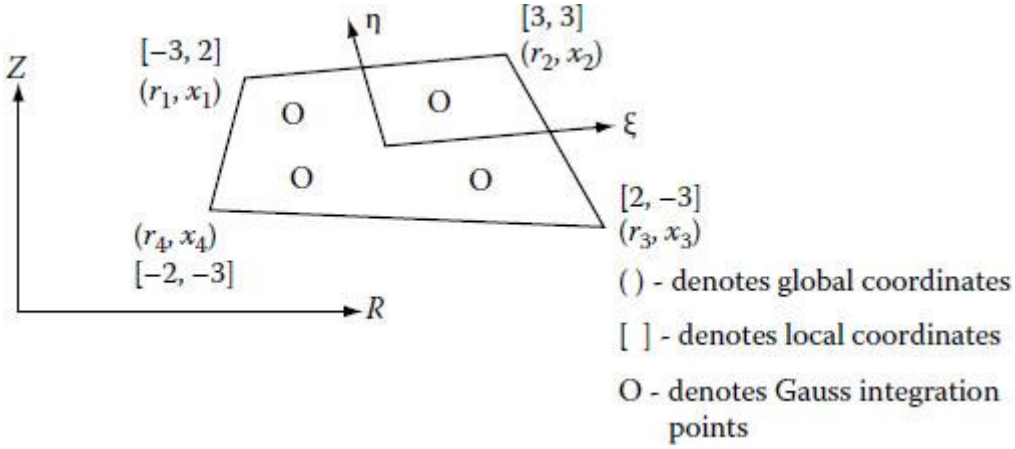

FIGURE 1.26
Illustration of isoparametric finite element and integration points.

$$[F] = [\mathbf{K}][\delta] \tag{1.48}$$

When the stiffness matrix, [**K**], of the foundation structure is available, one can use a linear algebraic solution scheme to solve for the unknown deflections and forces (such as reactions) with the known boundary conditions (deflections, δ, and forces, F). The solution technique is illustrated in Chapter 8 (Section 8.3.2.1).

1.9 Common Methods of Modeling Yielding Behavior of soils

Analytical solutions to foundation engineering problems, regardless of whether they are numerical or deterministic in their approach, must incorporate criteria for modeling the stress–strain behavior of foundation material as accurately as possible. Most geomateri-als exhibit nonlinear elastic properties at low stress levels, and therefore elastic methods described in Section 1.5 such as the Schmertmann method would provide reasonable esti mates of settlements at relatively low stress levels only. However, when relatively large loads are applied on a foundation, the foundation soils generally start to yield under these loads producing irrecoverable deformation. For instance, it is shown in Section 1.5 that low permeability soils such as clay and silt exhibit time-dependent irrecoverable consolidation, which cannot be modeled using the elastic or the incremental elastic theory. Furthermore, excessive settlements undergone by uncompacted coarse-grained soils such as loose and medium dense sand and gravel, due to rearrangement of particles, cannot be analytically predicted satisfactorily using the elastic or incremental the elastic theory alone.

In addition, if the analyst is equipped with a comprehensive stress–strain theory that could model the complete behavior of a loaded earthen structure from initial small defor mation stages through large deformation yielding to ultimate failure, the analyst would be able to extract vital design parameters that would be useful in the design of that earthen structure not only to satisfy strength limits but also the desired serviceability limits. Hence, foundation engineers have to use sophisticated constitutive (stress–strain) models that can model earthen structures, analytically or numerically (Equation 1.37). Two such popular models—(1) modified Cam-clay model for clays and (2) Cap model that is typically used for granular soils—will be discussed in the ensuing sections. However, the effective application of any constitutive model to predict the behavior of an earthen struc ture accurately, depends on the fulfillment of the following experimental tasks:

1. Appropriate laboratory testing to determine the specific material parameters needed to execute the theoretical model
2. Field pilot testing based on scale models or prototypes themselves, to verify the analytical or numerical predictions for actual field applications, and perhaps to further calibrate the analytical model

1.9.1 Modified Cam-Clay Model

The modified Cam-clay model is based on research performed by Roscoe et al. (1963) and Roscoe and Burland (1968). It has been successfully applied in many field applications involving deformation of soft clays. In this theory, the isotropic consolidation behavior of clays is approximated by the following relationships.

1.9.1.1 Isotropic Consolidation of Clays

The following terminology applies to Figure 1.27. The mean normal effective stress, p is defined by

$$p = \frac{1}{3}(\sigma'_1 + 2\sigma'_3), \tag{1.49}$$

where a'_1 and a'_3 are the major and minor principal effective stresses, respectively. It is seen that under laboratory triaxial conditions (Section 1.4), the above stresses correspond respectively to axial and cell pressures. The specific volume (v) is defined as 1 + void ratio or 1 + e.

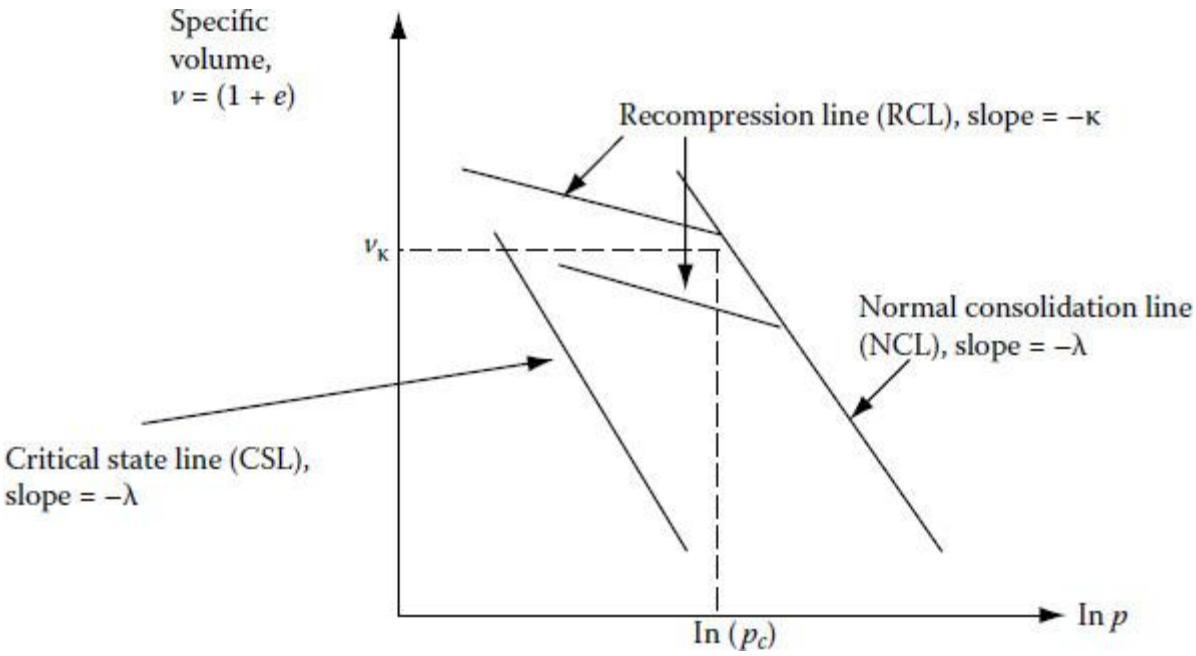

FIGURE 1.27
Isotropic consolidation parameters for modified Cam-clay model.

Then, the standard equation of the normal consolidation line (NCL) is

$$\upsilon = N - \lambda \ln(p) \tag{1.50}$$

Similarly, the standard equation of any recompression line (RCL) is

$$\upsilon = \upsilon_\kappa - \kappa \ln(p) \tag{1.51}$$

where v_K is the specific volume at the start of recompression, and N, κ, and λ are model parameters that can be obtained from laboratory isotropic consolidation tests performed using the triaxial cell. During isotropic consolidations tests, the clay sample is compressed under 3-D stress conditions as compared to conventional 1-D tests. Figure 1.27 also shows that there are an infinite number of RCLs that form a family of RCLs for different v_K values. Figure 1.27 also shows how v_K can be related to the overconsolidation ratio (OCR) that is characteristic of each RCL. OCR is defined as the ratio of the maximum past effective pres sure (p_c in Figure 1.27) to the current effective pressure as

$$\upsilon_\kappa = N - (\lambda - \kappa)\ln[(\mathrm{OCR})p_0] \tag{1.52}$$

or

$$\upsilon_\kappa = N - (\lambda - \kappa)\ln[p_c] \tag{1.53}$$

It is important to realize that the deformation behavior of OC clay within a given RCL is strictly elastic. However, plastic deformations occur if the stress path corresponding to a spe cific loading situation displaces the stress-volume state of an OC sample onto a different RCL.

It must also be noticed that λ and κ are the 3-D equivalents of C_c and C_r in Equation 1.18 and Figure 1.19.

1.9.1.2 Critical State of Deformation of Clay

Shear strength testing of clays under triaxial (Section 1.4) or direct shear conditions indicate that the ultimate failure occurs at a *critical state* where excessive shear deformation occurs with no further change in the stress conditions, that is, shear or mean normal effective stress. This final state reached by the sample is a unique state for a given clay type independent of the initial consolidation state, that is, normal consolidation (NC) or overconsolida-tion (OC) of the clay sample, and the drainage condition that exists during shearing, that is, drained (CD) or undrained (CU). If the shear stress is defined by the following expression

$$q = \sigma'_1 - \sigma'_3 \tag{1.54}$$

then, the critical state line can be depicted on a *q–p* plot, as shown in Figure 1.28.

The equation of the CSL can be expressed as

$$q = Mp, \tag{1.55}$$

where M is another modified Cam-clay model parameter that can be obtained from any triaxial test performed on a sample from that clay.

The stress state of a typical soil sample that exists in the field can be represented by the K_o condition described in Chapter 10 (Equations 10.5 and 10.6). In order to better visualize the gradual deformation of a field clay sample starting under K_o conditions (Figure 1.28) until it ultimately reaches the critical state line and fails, its combined stress and volumetric strain path can be plotted on a 3-D *q–p–v* plot, as shown in Figure 1.29. Figure 1.29 also shows that the stress and volumetric deformation states of clays are bounded by a convex surface known as the state boundary surface (SBS) and a ruled Hvorslev surface, on both of which yielding can take place. The CSL defines the boundary of the above two surfaces. Therefore, CSL is, in fact, a line in 3-D space the corresponding q–p projection of which is shown in Figure 1.28.

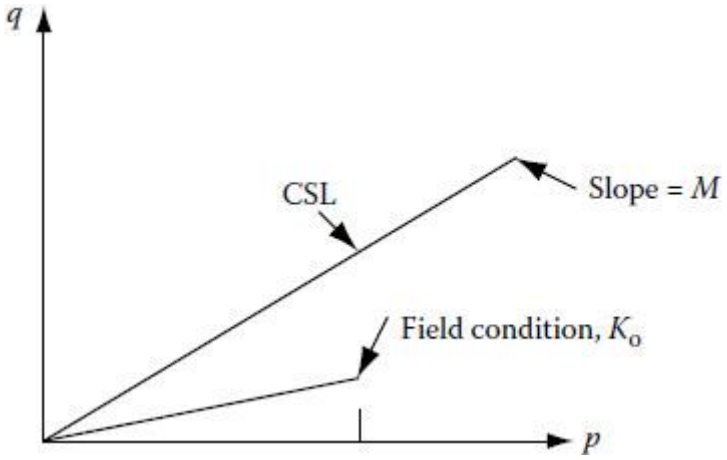

FIGURE 1.28
Illustration of critical state line and field stress state of a clay layer.

The equation of the CSL projection on *v–p* is given by (Figure 1.28)

$$\upsilon = N - (\lambda - \kappa)\ln 2 - \lambda \ln(p) \tag{1.56}$$

Therefore, in 3-D space, the CSL is a line represented by both Equations 1.55 and 1.56.

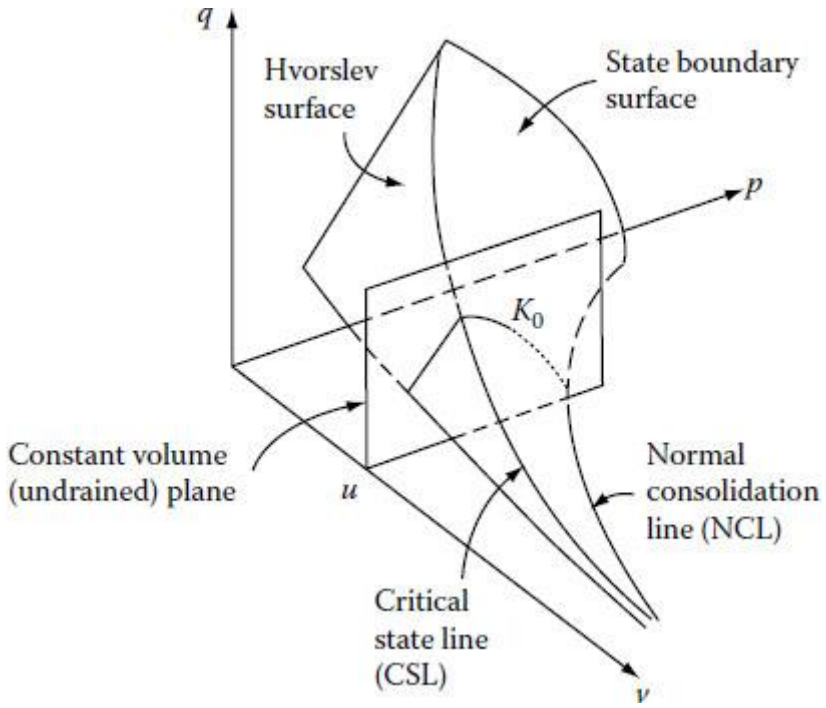

FIGURE 1.29
Three-dimensional representation of deformation of clay up to failure.

On the other hand, the equation of the Hvorslev surface (Figure 1.29) can be expressed as follows (Schofield and Worth, 1968):

$$q = (M - h)e^{\left[\frac{N-(\lambda-\kappa)\ln 2-\upsilon}{\lambda}\right]} + hp \tag{1.57}$$

where h, which defines the (constant) slope of the ruled Hvorslev surface on the q–p plane, is another material constant that can be determined from triaxial tests. Furthermore, the equation of the SBS (Figure 1.29) can be expressed as (Schofield and Worth, 1968)

$$\upsilon = N - (\lambda - \kappa)\ln\left(p + \frac{q^2}{M^2 p}\right) - \kappa \ln(p) \tag{1.58}$$

The following observations are made based on Figure 1.29:

1. Stress states of normally consolidated (NC) clays plot on the SBS.
2. Under undrained shearing, NC clays start from K_o conditions on SBS and exhibit strain hardening behavior (path 1 in Figure 1.30) until failure on the CSL.
3. Under undrained shearing, slightly OC clays start from K_o conditions immediately inside the SBS and exhibit strain hardening behavior (path 2 in Figure 1.30) up to the SBS and subsequently strain harden further until they reach failure on the CSL.
4. Under undrained shearing, highly OC clays start from K_o conditions well inside the SBS and exhibit strain hardening behavior (path 3 in Figure 1.30) up to the Hvorslev surface and subsequently strain harden further until failure is reached on the CSL.
5. Under shearing, OC samples exhibit elastic behavior until they approach either the SBS or the Hvorslev surface depending on the OCR. Therefore, during und-rained shearing

with the specific volume v remaining constant, the only way in which clays can retain their elastic properties without moving onto a different RCL is to retain the same mean effective stress, p. Hence, undrained stress paths of OC clays remain vertical until they approach either the SBS or the Hvorslev surface (Figure 1.30).

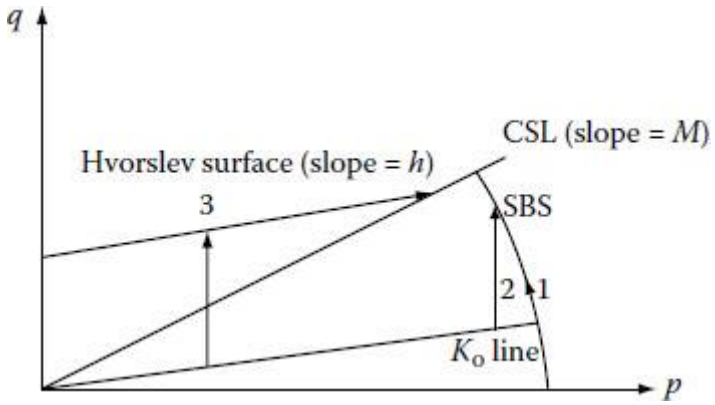

FIGURE 1.30
Undrained stress paths of field clay samples.

TABLE 1.12
Laboratory Evaluation of Modified Cam-Clay Model Parameters

Model Parameter	Laboratory Test	Type of Sample
M	Triaxial (CU or CD)	NC or OC
λ	Isotropic consolidation	NC
N	Isotropic consolidation	NC
K	Isotropic consolidation	OC
h	Triaxial (CU)	OC

The preceding discussion illustrates that the SBS and Hvorslev surfaces can be considered yield surfaces in the study of plastic behavior of clays.

1.9.1.3 Stress–Strain Relations for Yielding Clays

The normality condition or the *associated flow rule* in plastic theory states that the plastic flow vector (for 2-D yield surfaces) is normal to the yield surface at the stress point corresponding to any stress state. By assuming the normality condition, Roscoe and Burland (1968) derived the following plastic stress–strain relationship for clay yielding on the SBS.

$$\begin{bmatrix}\Delta\varepsilon_p\\ \Delta\varepsilon_q\end{bmatrix} = \frac{\lambda-\kappa}{\upsilon p(M^2+\eta^2)}\begin{bmatrix}M^2-\eta^2 & 2\eta\\ 2\eta & \frac{4\eta^2}{M^2-\eta^2}\end{bmatrix}\begin{bmatrix}\Delta p\\ \Delta q\end{bmatrix}, \tag{1.59}$$

where $\eta = q/p$ represents the current stress state on the SBS. Equation 1.59 amply illustrates the *shear–volume coupling* phenomenon or the occurrence of volumetric strains as well due to shearing stresses. This is particularly noticeable in the case of granular material such as medium dense and

dense sands, for which more applicable stress–strain models are discussed in Sections 1.9.2 and 1.9.3.

The usefulness of relationships such as Equation 1.59 is that they can be used conveniently in the [**D**] matrix of the FE formulation (Section 1.8) providing a convenient mechanism to incorporate plastic deformation in finite element modeling of foundation problems. Table 1.12 shows the model parameters that must be evaluated for calibration of the modified Cam-clay model and the appropriate laboratory tests that can be used for the evaluation.

An example problem on the modified Cam-clay model is solved in Example 1.9 at the end of this chapter.

1.9.2 Cap Model

The Cap model, more appropriately considered as a collection of many models, is based on concepts introduced by Drucker et al. (1957) and further developed by DiMaggio and Sandler (1971). This model has been used to represent both the mechanical behavior of many geologic materials, including sand, clay, and rock under high and low pressure conditions. As shown in Figure 1.31 and mathematically represented in Equations 1.62 through 1.69, the cap model consists of a strain hardening elliptical cap and an elastic perfectly plastic Drucker–Prager failure surface plotted on a p (mean normal effective stress) versus q (deviator stress) plot. Although the p-versus-q plot in Figure 1.31 is adequate to represent *triaxial stress* states, the *generalized cap model* must be plotted on the Inversus- $\sqrt{J_2}$ plot, where I_1 and J_2 are the first invariant of the stress tensor (Equation 1.60) and second invariant of the deviatoric stress tensor (Equation 1.61), respectively.

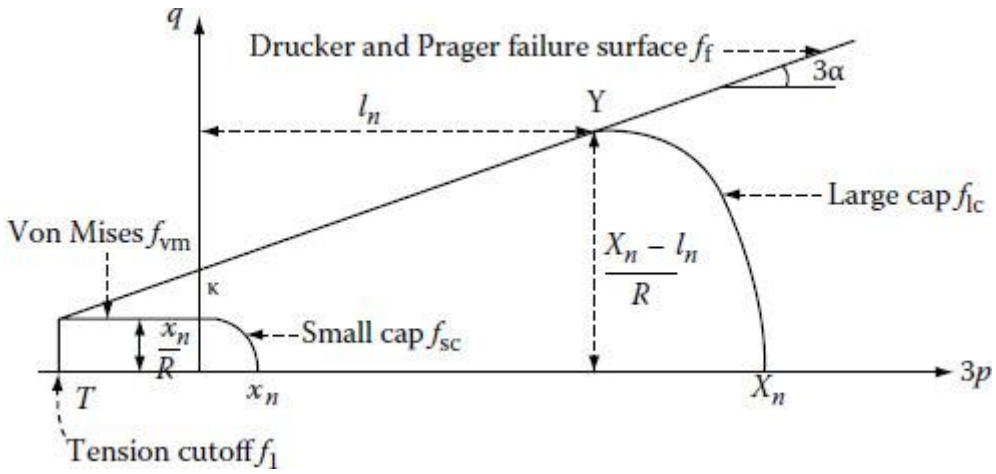

FIGURE 1.31
Illustration of the Cap model.

$$I_1 = \sigma_x + \sigma_y + \sigma_z \tag{1.60}$$

$$J_2 = (\sigma_x - \sigma_y)^2 + (\sigma_y - \sigma_z)^2 + (\sigma_z - \sigma_x)^2 + 6(\tau_{xy}^2 + \tau_{yz}^2 + \tau_{zx}^2), \tag{1.61}$$

where σ and τ represent the normal and shear stresses on the x, y, and z planes.

For triaxial (axisymmetric) stress states, it is seen from Equations 1.60 and 1.61 that $I_1 = 3p$ and $\sqrt{J_2} = q$.

In the cap model, the soil behavior is assumed to be linear elastic inside the yield surface, whereas on the yield surface, soils are assumed to deform plastically based on an associative flow rule as in the case of the Cam-clay model discussed in Section 1.9.1. The Cap model has widespread use as a constitutive model in many FE computational methodologies used in earthen structure design. This is primarily because the presence of the strain hardening cap provides a facility to model the shear-induced dilatancy behavior of overconsolidated clays and dense sands and similarly the shear-induced compression behavior of normally consolidated clays and loose sands.

The mathematical representation of the cap model is described below.

Drucker and Prager failure surface (f_f)

$$3\alpha p + q - k = 0 \tag{1.62}$$

von Mises failure surface (f_{vm})

$$q + x_n / R = 0 \tag{1.63}$$

Elliptical hardening caps: large cap (f_{lc})

$$(3p - l_n)^2 + R^2 q^2 - (X_n - l_n)^2 = 0 \tag{1.64}$$

Small cap (f_{sc})

$$(3p)^2 + R^2 q^2 - x_n^2 = 0 \tag{1.65}$$

Tension cutoff (f_1)

$$3p - T = 0 \tag{1.66}$$

where

$$X_n = \frac{1}{D} \ln\left(1 + \frac{\varepsilon_v^p}{W}\right) \tag{1.67}$$

$$\alpha = \frac{2\sin\phi}{\sqrt{3}(3-\sin\phi)} \tag{1.68}$$

$$k = \frac{6c(\cos\phi)}{\sqrt{3}(3-\sin\phi)} \tag{1.69}$$

D, *W*, and *R* are soil parameters

$$\varepsilon_v^p \text{ is the accumulated plastic volumetric strain} = \sum d\varepsilon_v^p \tag{1.70}$$

It is noted that the plastic volumetric strain is accumulated only if the stress (p) and strain increments are both compressive. The parameter l_n is limited to negative values to avoid development of tension. For positive l_n values, a modified small cap is assumed in the compressive stress range together with the von Mises failure surface as shown in Figure 1.31. If the maximum tensile stress that the soil can take, T, is known, then a tension cutoff can also be introduced as shown in Figure 1.31.

The above relationships can be used to express the plastic normal and shear strains $\Delta\varepsilon_{\rho}$ and $\Delta\#_{q}$ in terms of the stress increments Δp and Δq and form the corresponding [**D**] matrix in a relevant finite element formulation (Section 1.8) as in the case of the Cam-clay model (Equation 1.59). The main advantage of using such stress–strain models in finite element modeling of foundations is that they furnish a convenient mechanism to include the plastic deformation of soils in design considerations enabling the formulation of more realistic and economic design methodolgies. Table 1.13 shows the model parameters that must be evaluated for calibration of the Cap model and the appropriate laboratory tests that can be used for the evaluation.

1.9.3 Nonlinear Elastic Stress–Strain Relations

Another stress–strain relationship used popularly to model foundation soils in finite element formulations is the nonlinear elastic shear stress-shear strain model developed by

TABLE 1.13

Laboratory Evaluation of Cap Model Parameters

Model Parameter	Laboratory Test	Type of Soil
D	Isotropic consolidation	NC clay
		Loose sand
α	Triaxial (CU or CD)	NC clay
		Loose sand
k	Triaxial (CU or CD)	NC clay
		Loose sand
R	Triaxial (CU)	OC/NC clay
		Loose/dense sand
W	Isotropic consolidation	NC clay
		Loose sand
T	Triaxial extension	OC clay
		Dense sand

Hardin and Drnevich (1972). This can be mathematically expressed in Equation 1.71 and plotted on a stress–strain plot as shown in Figure 1.32.

$$\tau = \frac{\gamma}{1/G_{\max} + \gamma/\tau_{\max}}, \tag{1.71}$$

where $G_{\max}$ and $T_{\max}$ are the initial shear modulus and the maximum shear stress, respectively, as shown in Figure 1.32. It can be seen in Figure 1.32 that the instantaneous (or tangential) shear modulus decreases in magnitude with increasing shear and $G_{\max}$ can also be interpreted as the shear modulus under very low strain levels. Equation 1.71 is of special significance when the response of soils is analyzed under dynamic loading conditions.

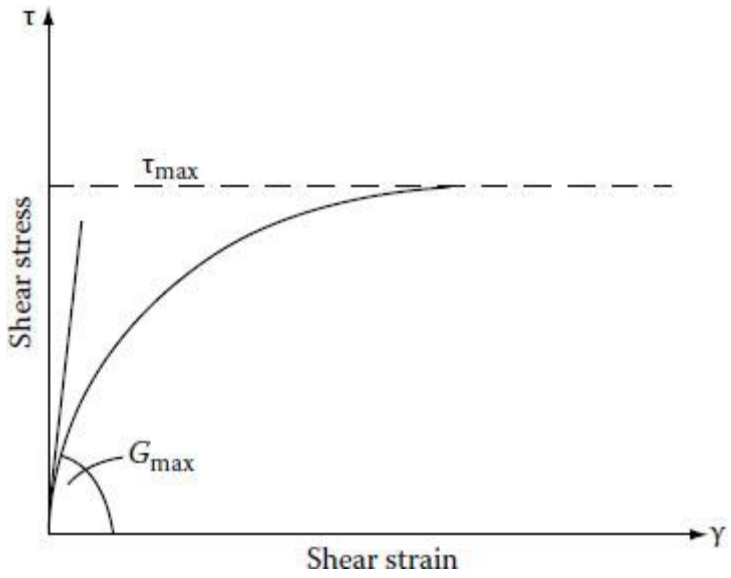

FIGURE 1.32
Nonlinear elastic relationship.

1.9.3.1 Evaluation of Nonlinear Elastic Parameters

The nonlinear elastic stress–strain parameters G_{max} and T_{max} can be determined from direct shear and simple shear tests under static loading conditions and cyclic simple shear tests under dynamic loading conditions. For direct shear conditions, the failure plane is predefined to be horizontal. Hence, T_{max} can be evaluated using the Mohr-Coulomb criterion in Equation 1.6,

$$\tau = c + \sigma \tan\phi, \tag{1.6}$$

where σ is the normal stress applied during a direct shear test. In the case of simple shear tests, the plane where the normal and shear stresses fit Equation 1.6 automatically becomes the failure plane. In such cases, T_{max} can be determined conveniently using a Mohr circle construction.

Analytical expressions are also available for evaluating G_{max}. For example, G_{max} for sandy soils can be expressed by the following expression:

$$G_{max} = A\frac{(B-e)^2}{1+e}\bar{\sigma}_0^{1/2}, \tag{1.72}$$

where $\bar{\sigma}_0$ is the mean normal stress (Equation 1.9) and e is the void ratio. When G_{max} and $\bar{\sigma}_0$ are measured in kPa, the values of A and B are as follows:

For round-grained sands, A = 6908 and B = 2.17
For angular-grained sands, A = 3230 and B = 2.97

On the other hand, in the case of clays, the following modified form of Equation 1.72 presented by Hardin and Drnevich (1972) can be used to evaluate G_{max} from basic index and consolidation properties as well as the state of stress.

$$G_{max} = A\frac{(B-e)^2}{1+e}(\mathrm{OCR})^K\bar{\sigma}_0^{1/2}, \tag{1.73}$$

where G_{max} and σ_0 are both expressed in kPa. Furthermore,

$A = 3230$, $B = 2.97$ and
$K = 0.4 + 0.007(\text{PI})$ for $0 < \text{PI} < 40$

and

$K = 0.68 + 0.001(\text{PI} - 40)$ for $40 < \text{PI} < 80$
OCR = overconsolidation ratio
PI = plasticity index

1.9.3.2 *Evaluation of G_{max} from Standard Penetration Tests*

Seed (1986) presented the following correlation between G_{max} and the SPT blow count (Section 2.4.1).

$$G_{\max} = 5654(N_{60})^{0.34}\bar{\sigma}_0^{0.4}, \tag{1.74}$$

where G_{max} and σ_0 are both expressed in kPa.

N_{60} is the SPT blow count obtained with an SPT setup that delivers 60% of the theoretical free-fall energy of the hammer to the drill rod.

1.9.4 Concepts of Stress-Dilatancy Theory for Granular Soils

In contrast to the popular approach of incorporating stress–strain relations for soils assuming a linear elastic (Section 1.5.1), nonlinear-elastic (Section 1.9.3), elasto-plastic (Sections 1.9.1 and 1.9.2) continua, particulate mechanics has also been used to explain the behavior of soils, especially in the case of sands. Stress dilatancy theory (Rowe, 1963) is a result of the research conducted toward understanding the deformation of soils as discrete particulate matter. The following assumptions form the framework of this theory:

1. During deformation of soils particles tend to slide much more frequently than rolling.
2. The individual particles are rigid and hence they cannot contribute an elastic component toward deformation.
3. Instant sliding is confined to some preferred angle. The following expression can be used to describe the stress–strain relationship at a given stress level:

$$\frac{\sigma'_1}{\sigma'_3} = \left[\frac{1-\frac{du}{dy}}{1+\frac{du}{dy}}\right]\left[\tan^2(45 + \phi_{cv}/2)\right], \tag{1.75}$$

where $\#_{cv}$ is the angle of friction under large shear strains where shearing would occur under constant volume.

The principal stress ratio under triaxial conditions, $\frac{\sigma'_1}{\sigma'_3}$, can be related to the developed angle of friction # as;

$$\frac{\sigma'_1}{\sigma'_3} = \tan^2(45 + \phi/2) \tag{1.76}$$

and the rate of volume change with respect to shear strains at a constant confining pres sure, $dv/d\gamma$, can be expressed in terms of the dilation angle, ν, as;

$$\frac{d\upsilon}{d\gamma} = -\sin\nu \tag{1.77}$$

Inspection of Equation 1.75 shows that when shearing occurs in granular soils without any volumetric strains ($dv/d\gamma = 0$), then # = $\#_{cv}$.

On the other hand, according to this theory, in the case of dense or medium dense sands, shear failure would occur at maximum dilation conditions (Figure 1.33). Under those conditions, the developed angle of friction will be equal to the angle of interparticle friction, or # = $\#_f$

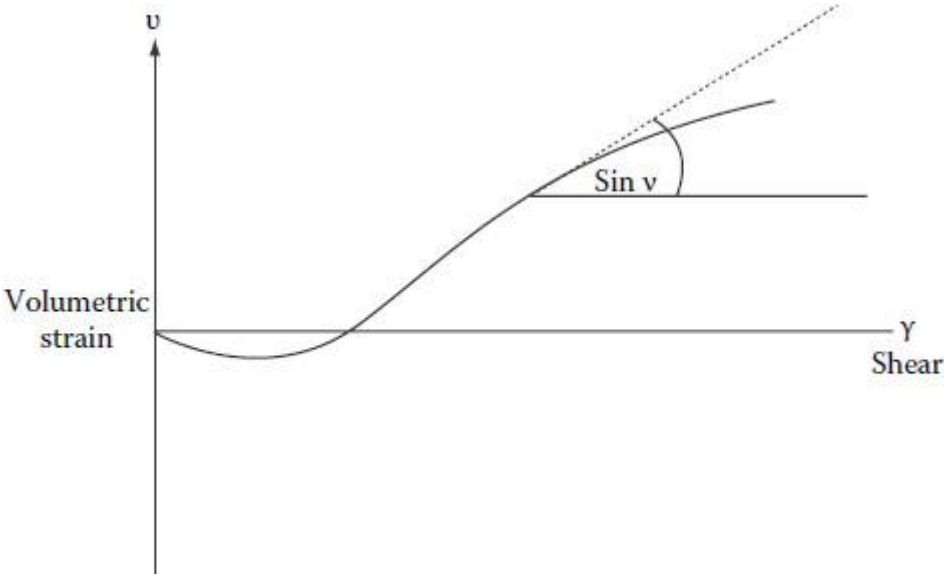

FIGURE 1.33
Shear dilatation of granular soils.

This condition will also correspond to the occurrence of the maximum principal stress ratio, $\left[\frac{\sigma'_1}{\sigma'_3}\right]_{max}$

Equation 1.75 can also be arranged to fit the **[D]** matrix of the finite element formulation (Section 1.8), thus providing a mechanism to incorporate plastic deformation of granular soils in finite element modeling of foundation problems.

1.10 Additional Examples

Example 1.8: Unsaturated Soils Mechanics

Use the parameters provided in Table 1.11 for to plot the variation of volumetric water content with matric suction for an unsaturated fine sand located 6 m below the ground level. Use the plot to estimate

(a) Its gravimetric moisture content (m) at a suction of 100 kPa if the degree of saturation is 50%
(b) Its air pressure, if the water pressure is known to be 15 kPa
(c) Its effective stress, if the x parameter is assumed to be 0.5

Solution

Substitution of the parameters in Table 1.11 in Equations 1.29 and 1.30 yields

$$\theta = C(\psi)\frac{0.45}{\left\{\ln\left[2.718+\left(\frac{\psi}{1.948}\right)^{2.708}\right]\right\}^{1.084}},$$

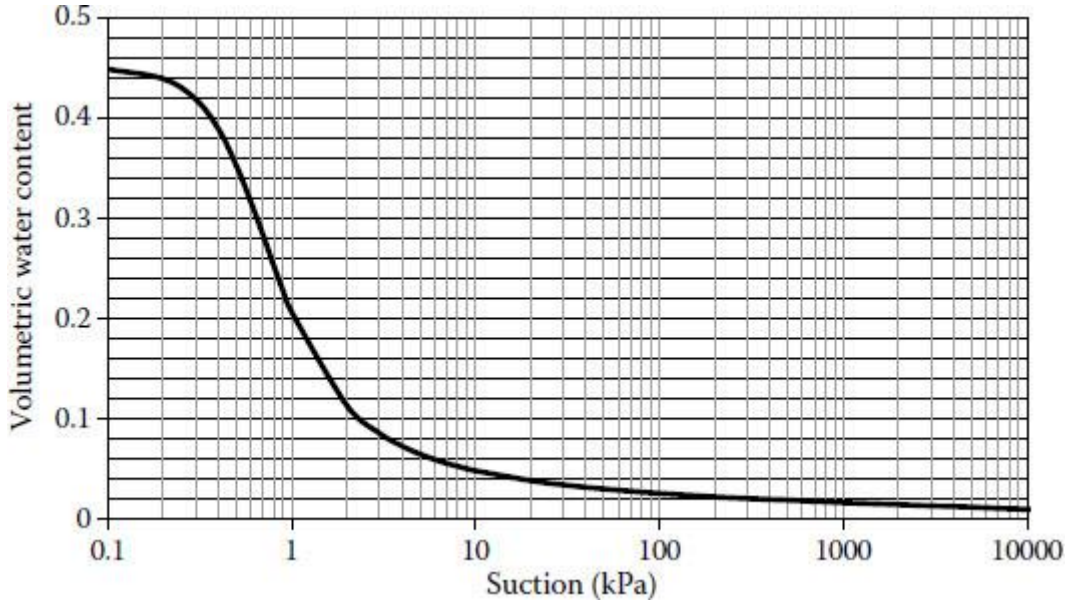

FIGURE 1.34

Soil-water characteristic curve for fine sand. where

where

$$C(\psi) = \frac{-\ln\left(1+\frac{\psi}{30}\right)}{\ln\left[1+\left(\frac{10^6}{30}\right)\right]} + 1$$

The required plot is shown in Figure 1.34.

(a) In Figure 1.34, volumetric water content at a suction of 100 kPa, θ = 0.03 The degree of saturation = 0.5 = $V_w/(V_a + V_w)$, yielding $V_a = V_w$
Using Equation 1.28, 0.03 = Vw/V = V**w**/V**a** + V**w** + V_s) = V**w**/(2V**w** + V_s) The above result yields V_w/V_s = 0.032
If one uses the respective specific gravities of water and solids, that is, 1 and 2.65 respectively in the above result, one obtains W**v**/(1)/W**s**/(2.65) = 0.032
2.65W_w/W_s = 0.032, yielding a gravimetric moisture content (W_w/W_s) of 1.2%
(b) Suction = u_a - u_w = 100 kPa Since u_w = 15 kPa u**a** = 115 kPa
(c) Assuming the average unit weight of soil to be 18 kN/m^3, Equation 1.27 can be used to estimate the effective stress in that soil sample as

$$\sigma' = 5(18) - 115 + (0.5)(100) = 25\text{kPa}$$

Example 1.9: Modified Cam-Clay Model

An NC clay sample retrieved from a depth of 2.5 m in an embankment yielded the following (drained) triaxial and consolidation test parameters in the laboratory.

1. Mohr-Coulomb friction = 20°
2. Slope of isotropic virgin consolidation line = 0.3

3. Slope of isotropic virgin RCL = 0.05
   (a) Estimate the modified cam-clay parameters.
   (b) Assuming that the void ratio of the sample is 0.9, develop the instantaneous stress–strain relationship to be used in a finite element model to predict its deformation.

Solution

Using the definitions of q (Equation 1.54) and p (Equation 1.49) in Equation 1.55, one obtains

$$(\sigma_1 - \sigma_3) = (1/3)M(\sigma_1 + 2\sigma_3)$$

The above results can be algebraically simplified to obtain the corresponding Mohr–Coloumb plot as

$$(\sigma_1 - \sigma_3) = (3M/6 + M)(\sigma_1 + \sigma_3)$$

However, it is known that the critical state line is equivalent to the Coloumb failure line on the Mohr-Coloumb plot. Thus,

$$(\sigma_1 - \sigma_3) = (\sin\phi)(\sigma_1 + \sigma_3)$$

It follows that sin φ = (3M/6 + M)

(a)

In this example, since φ = 20°, M = 0.77

From the given data and Equation 1.50, λ = 0.3

From the given data and Equation 1.50, κ = 0.05

Specific volume, $v = 1 + e$ = 1.9

(b)

Principal effective stresses at a depth of 2.5 m can be found as follows by assuming a unit weight of 18 kN/m^3, and that there are neither shear forces on the vertical and horizontal planes nor groundwater above the considered location. From Equation 10.6 (Chapter 10),

ssuming NC clay and OCR = 1)

$5)(18) = 45(1 - K_0) = 15.3\text{kPa}$

$$3)(\sigma_1 + 2\sigma_3) = 45(1 + 2K_0)$$

$$p = 3(1 - K_0)$$

Substituting all the above values in Equation 1.59,

$$\begin{bmatrix}\Delta\varepsilon_p\\ \Delta\varepsilon_q\end{bmatrix} = \frac{0.3-0.05}{(1.9)(34.8)(0.77^2+44^2)}\begin{bmatrix}0.77^2 - 0.44^2 & 2(0.44)\\ 2(0.44) & \frac{4(0.44)^2}{0.77^2-0.44^2}\end{bmatrix}\begin{bmatrix}\Delta p\\ \Delta q\end{bmatrix}$$

$$\begin{bmatrix}\Delta\varepsilon_p\\ \Delta\varepsilon_q\end{bmatrix} = 4.81\begin{bmatrix}0.4 & 0.88\\ 0.88 & 1.94\end{bmatrix}\begin{bmatrix}\Delta p\\ \Delta q\end{bmatrix}$$

References

Bishop, A.W., and Blight, G.E., 1963. Some aspects of effective stress saturated and unsaturated soils. *Geotechnique*, 13: 177-197.

Bowles, J.E., 1986. *Engineering Properties of Soils and Their Measurements*. McGraw-Hill, New York.

Bowles, J.E., 2002, *Foundation Analysis and Design*. McGraw-Hill, New York.

Clifton, A.W., Barbour, S.L., and Wilson, G.W., 1999. *The Emergence of Unsaturated Soil Mechanics: Fredlund Volume*. NRC Research Press, Ottawa, Ontario, Canada.

Das, B.M., 2002. *Soil Mechanics Laboratory Manual*. Oxford University Press, New York.

D'Appolonia, D.J. et al., 1970. Closure: Settlement of spread footing on sand. *J Soil Mech Found Eng ASCE* 96 (SM2): 754–762.

DiMaggio, F.L., and Sandler, I.S., 1971. Material models for granular soils. *J Eng Mech Div ASCE* 97(EM3): 935–950.

Drucker, D.C., Gibson, R.E., and Henkel, D.J., 1957. Soil mechanics and work-hardening theories of plasticity. *Trans ASCE* 122: 338–346.

Fredlund, D.G., and Morgenstern, N.R., 1977. Stress state variables for unsaturated soils. *J Geotech Eng Div ASCE* 103(GT5): 447–466.

Goodman, R.E., 1989. *Introduction to Rock Mechanics*. Wiley, New York.

Hardin, B.O., and Drnevich, V.P., 1972. Shear modulus and damping in soils: Design equations and curves. *J Soil Mech Found Div ASCE* 98(SM7): 667–692.

Holtz, R.D., and Kovacs, W.D., 1981. *An Introduction to Geotechnical Engineering*. Prentice Hall, Englewood Cliffs, NJ.

Hughes, T.J.R., 1987. *The Finite Element Method*. Prentice Hall, Englewood Cliffs, NJ.

Lam, L., Fredlund, D.G., and Barbour, S.L., 1987. Transient seepage model for saturated-unsaturated soil systems: A geotechnical engineering approach. *Can Geotech J* 24: 565–580.

Lu, N., and Likos, W.J., 2004. *Unsaturated Soil Mechanics*. Wiley, New York.

Roscoe, K.H., and Burland, J.B., 1968. On the generalized stress–strain behavior of 'wet' clay. In: Heyman, J., and Leckie, F.A. (eds.) *Engineering Plasticity*. Cambridge University Press, Cambridge.

Roscoe, K.H., Schofield, A.N., and Thurairajah, A., 1963. Yielding of clays in states wetter than critical. *Geotechnique* 13: 211–240.

Rowe, P.W., 1963. The stress dilatancy relation for static equilibrium of an assembly of particles in contact. *Proc R Soc Soil Mech Found Eng* A269: 500–527.

Schmertmann J.H., and Hartman, J.P., 1978. Improved strain influence factor diagrams. *J Geotech Eng Div Am Soc Civil Eng* 104(GT8): 1131–1135.

Schofield, A.N., and Wroth, C.P., 1968. *Critical State Soil Mechanics*. McGraw-Hill, New York.

Seed, H.B., Wong, R.T., Idriss, I.M., and Tokimatsu, K., 1986. Moduli and damping factors for dynamic analysis of cohesive soils. *J Geotech Engr ASCE* 112 (GTII): 1016–1032.

Wray, W., 1986, *Measuring Engineering Properties of Soils*. Prentice Hall, Englewood Cliffs, NJ.

Zienkiewicz, O.C., Humpheson, C., and Lewis, R.W., 1977, A unified approach to soil mechanics problems (including plasticity and visco-plasticity. In: Gudehus, G. (ed.) *Finite Element in Geomechanics*. Wiley, New York.